

Energy Efficient Dual-Functional Radar-Communication: Rate-Splitting Multiple Access, Low-Resolution DACs, and RF Chain Selection

Onur Dizdar, *Member, IEEE*, Aryan Kaushik, *Member, IEEE*, Bruno Clerckx, *Fellow, IEEE*,
and Christos Masouros, *Senior Member, IEEE*

Dual-Functional Radar-Communication systems enhance the benefits of communications and radar sensing by jointly implementing these on the same hardware platform and using the common RF resources. An important and latest concern to be addressed in designing such Dual-Functional Radar-Communication systems is maximizing the energy-efficiency. In this paper, we consider a Dual-Functional Radar-Communication system performing simultaneous multi-user communications and radar sensing, and investigate the energy-efficiency behaviour with respect to active transmission elements. Specifically, we formulate a problem to find the optimal precoders and the number of active RF chains for maximum energy-efficiency by taking into consideration the power consumption of low-resolution Digital-to-Analog Converters on each RF chain under communications and radar performance constraints. We consider Rate-Splitting Multiple Access to perform multi-user communications with perfect and imperfect Channel State Information at Transmitter. The formulated non-convex optimization problem is solved by means of a novel algorithm. We demonstrate by numerical results that Rate Splitting Multiple Access achieves an improved energy-efficiency by employing a smaller number of RF chains compared to Space Division Multiple Access, owing to its generalized structure and improved interference management capabilities.

Index Terms—Digital-to-analog converters, dual-functional radar-communication, energy-efficiency, rate-splitting multiple access, RF chain optimization

I. INTRODUCTION

THE increasing user demand for cellular services and wireless communication systems has congested the existing sub 6-GHz frequency spectrum. In Cisco's annual report, it is expected that there will be over 70% mobile users of the world population by 2023 with 5.3 billion internet users [1]. As per the Ericsson mobility report [2], video traffic will increase to 77% in 2026 and the number of IMS voice subscriptions will reach to 6.8 billion by 2026. This leads the demand to seek for either widely unused spectrum such as millimeter wave for the fifth generation (5G) wireless systems [3] or reusing/sharing of the spectrum used for other applications and systems such as radar technology. For instance, the sub 6-GHz spectrum allocated to radar systems can be made available for sharing between radar and wireless systems [4], [5].

The increased demand for connectivity, data and spectrum also lead to an increased demand for energy required to enable such massive networks. An approach to tackle the energy demand problem is to prioritize and investigate energy-efficient transmission and networking algorithms in next generation communications standards [6], [7]. Achieving high Energy-Efficiency (EE) in communications is significantly important for operators as well as end-users. Consequently, EE has

become a highly important metric in transceiver and network architecture design for the next generation standards [8]–[10].

Integrated Sensing and Communication (ISAC) systems have been studied in recent literature to counter the issue of spectrum congestion problem and improve EE by having a single device transmitting instead of two devices. Indeed, it was demonstrated that such joint systems have advantages over the individually operating radar and communication systems [11]–[15]. Integration of communications and radar functionalities is important in commercial systems as well as military systems, with applications in areas such as automotive radars and vehicular communications [16], [17]. There are two types of ISAC systems: the radar-communication co-existence (RCC) which requires effective coordination between the communication and radar units [18], whereas the Dual Functional Radar-Communication (DFRC) systems share the same hardware and signal for conducting both the operations [17], [19], [20].

Managing the interference in DFRC systems is important for an improved system performance, which may otherwise suffer from performance degradation in terms of both radar and communications functionalities. The most common type of interference considered in DFRC system design is the interference between the communications and radar signals, which occurs as a result of combining two separate systems with different operational purposes. On the other hand, multi-user interference can also occur for communication users when the multiple antennas at transmitter are exploited for improved spatial-multiplexing gain by means of multi-user transmission without perfect Channel State Information at Transmitter (CSIT). Consequently, a communication user in a DFRC system is susceptible to interference from both radar signals and communications signals for other users.

In this work, we consider a multi-antenna DFRC system

This work was supported by the UK Engineering and Physical Sciences Research Council (EPSRC) Grant numbers EP/S026622/1 and EP/S026657/1, and the UK MOD University Defence Research Collaboration (UDRC) in Signal Processing.

Onur Dizdar and Bruno Clerckx are with the Department of Electrical and Electronic Engineering, Imperial College London, U.K. (e-mail: {o.dizdar, b.clerckx}@imperial.ac.uk).

Aryan Kaushik is with the School of Engineering and Informatics, University of Sussex, U.K. (e-mail: aryan.kaushik@sussex.ac.uk).

Christos Masouros is with the Department of Electronic and Electrical Engineering, University College London, U.K. (e-mail: c.masouros@ucl.ac.uk).

which performs simultaneous multi-user communications and radar sensing with low-resolution Digital-to-Analog Converters (DACs). Our aim is to perform energy-efficient joint communications and radar jamming by means of low-resolution DACs and only activating the optimal number of RF chains at each transmission. We consider Rate-Splitting Multiple Access (RSMA) for multi-user communications in our proposed DFRC system. RSMA is a multiple access scheme based on the concept of Rate-Splitting (RS) and linear precoding for multi-antenna multi-user communications. RSMA splits user messages into common and private parts, and encodes the common parts into one or several common streams while encoding the private parts into separate streams. The streams are precoded using the available (perfect or imperfect) Channel State Information at the Transmitter (CSIT), superposed and transmitted via the Multi-Input Multi-Output (MIMO) or Multi-Input Single-Output (MISO) channel [21].

RSMA manages multi-user interference by allowing the interference to be partially decoded and partially treated as noise at the receivers. RSMA has been shown to encompass and outperform existing multiple access schemes, i.e., Space Division Multiple Access (SDMA), Non-Orthogonal Multiple Access (NOMA), Orthogonal Multiple Access (OMA) and multicasting. RSMA has been shown to be flexible and robust by its capability to adapt to any interference level and surpass the performance of SDMA and NOMA under perfect and imperfect Channel State Information at Transmitter (CSIT) [21]–[25]. This implies that RSMA can play a big role in emerging ISAC in a congested environment subject to interference among communications users but also among radar and communications.

A. Literature Review

The sharing of RF spectrum and hardware resources by multiple systems has increased the importance of interference management among the communication users and radar targets in an energy-efficient manner. The works on precoder design with interference management for co-existing and co-located DFRC systems, such as [18], [26], [27], consider design metrics in terms of communications rate, Signal-to-Noise Power Ratio (SNR) or multi-user interference, without any discussions on hardware power consumption or EE.

For energy-efficient MIMO DFRC systems, one needs to take into account the hardware power consumption and reducing the RF transceiver components such as RF chains and associated DAC bits, which are power hungry components, in an optimal way. Hybrid analog-digital (HAD) beamforming is proposed for DFRC systems in [28] to reduce the number of RF chains. HAD beamforming reduces the hardware costs and improves EE by creating a trade-off with the system performance. It has been shown in [29]–[31] that optimally selecting the active RF chains for HAD beamforming in communications only systems can further improve EE while maintaining good spectral efficiency performance. Beside RF chain selection, taking into account the DAC-bit optimization is also beneficial for EE maximization [32]. For DFRC systems, it has been shown in [33] that RF chain selection can provide advantages

in terms of the hardware complexity with favourable radar beampattern performance. However, the investigated scenarios in [33] consider full-bit resolution sampling and does not tackle the interference management problem directly. Furthermore, [34] addresses the EE maximization in DFRC systems while considering low DAC-bit resolution sampling, however the issue of interference management is missing.

Recent works [35], [36] have tackled the interference management problem in MIMO DFRC systems by employing RSMA, however, without any considerations for EE or interference due to imperfect CSIT. In [37], [38], the authors deal with the sum-rate maximization of a DFRC system employing RSMA under imperfect CSIT, without considering the EE performance, low-resolution DACs or the problem of RF chain selection. In [39], the authors investigate a DFRC system with low-resolution DACs under a total transmit power constraint and compare the performance of RSMA with that of SDMA, again with perfect CSIT assumption. The results in [39] demonstrate the advantage of RSMA in systems considering power consumption by DACs, which provides a motivation to study RSMA in more advanced setups with RF chain selection, which can further reduce power consumption and increase EE.

B. Contributions

The main contributions of this work can be listed as follows:

- We propose a DFRC system model to perform multi-user communications and radar sensing simultaneously. The proposed system model considers the practical impairments resulting from low-resolution DACs and imperfect CSIT. We consider RSMA as the enabling technology in the proposed system. Our aim is to find the optimal precoders, message split into common and private streams, and active RF chains to operate with maximum EE. To the best of our knowledge, this is the first paper to consider RF chain selection for EE in a DFRC system with low-resolution DACs and RSMA.
- We formulate a non-convex optimization problem to find the optimal precoders and active RF chains. The formulated problem is an EE maximization problem under total power, constant modulus, communications performance and radar performance constraints. The communications performance is guaranteed by a Quality-of-Service (QoS) constraint, which imposes a minimum rate value for each user. The radar performance is guaranteed by limiting the norm of the covariance matrix of the designed waveform to a reference matrix. We propose alternative reference matrices to account for different radar operation modes, namely, detection and tracking modes.
- We propose an Alternating Optimization (AO) based algorithm to solve the formulated non-convex problem by iterating between subproblems which find the optimal precoders and active RF chains separately. The subproblem to find the optimal precoders is solved by an algorithm based on Alternating Direction Method of Multipliers (ADMM) method. The subproblem to determine the active RF chains is solved by an algorithm based on Successive Convex Approximation (SCA) and

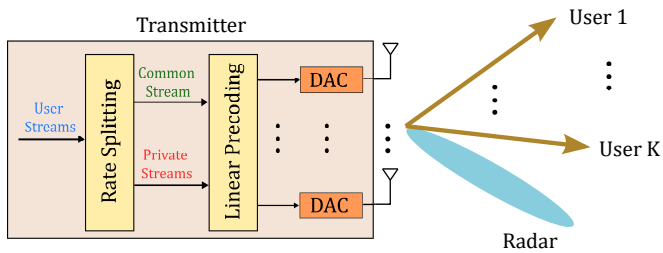


Fig. 1: System model.

Semi Definite Relaxation (SDR) methods. We prove the convergence of the overall proposed algorithm and provide an algorithmic complexity analysis.

- Numerical results demonstrate that RSMA can operate with a higher EE while achieving similar communications and radar performance, due its improved interference management capability and higher degrees-of-freedom in the precoder design space.

Notation: Vectors are denoted by bold lowercase letters and matrices are denoted by bold uppercase letters. The operations $|\cdot|$ and $\|\cdot\|$ represent the absolute value of a scalar and l_2 -norm of a vector, respectively. The notation \mathbf{a}^H denotes the Hermitian transpose of a vector \mathbf{a} . $\mathcal{CN}(0, \sigma^2)$ represents the Circularly Symmetric Complex Gaussian distribution with zero mean and variance σ^2 . \mathbf{I}_n represents the n -by- n identity matrix. $\mathbf{0}_n$ represents the all-zero vector of dimensions n -by-1. The operator $\text{Diag}(\mathbf{X}_1, \dots, \mathbf{X}_K)$ builds a matrix \mathbf{X} by placing the matrices $\mathbf{X}_1, \dots, \mathbf{X}_K$ diagonally and setting all other elements to zero. The operator $\text{diag}(\mathbf{X})$ builds a vector \mathbf{x} from the diagonal elements of \mathbf{X} . The operator $\text{vec}(\mathbf{X})$ vectorizes the matrix \mathbf{X} into a column vector by concatenating its columns.

The organization of the paper is as follows: Section II presents the system model. Section III gives the problem formulation and the proposed solution algorithm. Section IV extends the proposed formulation and solution algorithm to the imperfect CSIT case. Section V gives the numerical results. Section VI concludes the paper.

II. SYSTEM MODEL

We consider a Dual-Functional Radar-Communication (DFRC) system consisting of one transmitter with N_t transmit antennas serving K single-antenna users indexed by $\mathcal{K} = \{1, \dots, K\}$ while detecting a single target. Fig. 1 shows the considered system model. The transmitter performs joint communications and radar operation using RSMA. The modulated and precoded transmit signal is converted to analog by means of separate DACs connected to each of the transmit antennas. The transmitter transmits L consecutive samples in each Pulse Repetition Interval (PRI) of the radar system. We give the details of the system model in the following subsections.

A. Rate Splitting Multiple Access

RSMA is a multiple access technique that relies on linearly precoding at the transmitter and Successive Interference Cancellation (SIC) at the receivers. RSMA splits the user messages

into common and private parts, encodes the common parts of the user messages into a common stream to be decoded by all receivers, encodes the private parts of the user messages into private streams and superposes them in a non-orthogonal manner.

Let us denote the messages intended for the communication users as $W_k, \forall k \in \mathcal{K}$. The transmitter splits each user message into common and private parts, i.e., $W_{c,k}$ and $W_{p,k}$. The common parts of the messages, $W_{c,k}$, are combined into the common message W_c . The common message W_c and the private messages $W_{p,k}$ are independently encoded into streams s_c and $s_k, \forall k \in \mathcal{K}$, respectively. Linear precoding is applied to all streams with $\mathbf{P} = [\mathbf{p}_c, \mathbf{p}_1, \dots, \mathbf{p}_K]$, where $\mathbf{p}_c, \mathbf{p}_k \in \mathbb{C}^{n_t}$ are the precoders for the common stream and the private stream of the user- k , respectively. The communication signal at the transmitter is expressed as

$$\mathbf{x} = \mathbf{p}_c s_c + \sum_{k=1}^K \mathbf{p}_k s_k. \quad (1)$$

We assume that the streams have unit power, so that $\mathbb{E}\{\mathbf{s}\mathbf{s}^H\} = \mathbf{I}$, where $\mathbf{s} = [s_c, s_1, \dots, s_K]$. We assume that s_c and $s_k, \forall k \in \mathcal{K}$, are chosen independently from a Gaussian alphabet for theoretical analysis. The signal received by user- k user is written as

$$\mathbf{y}_k = \mathbf{h}_k^H \mathbf{x} + z_k, \quad \forall k \in \mathcal{K}, \quad (2)$$

where $\mathbf{h}_k \in \mathbb{C}^{n_t}$ is the channel vector and $z_k \sim \mathcal{CN}(0, \sigma_n^2)$ is the Additive White Gaussian Noise (AWGN) component for user- k .

The detection of the messages is carried out using the SIC algorithm. The common stream is detected first to obtain the common message estimate \hat{W}_c by treating the private streams as noise. The common stream is then reconstructed using \hat{W}_c and subtracted from the received signal. The remaining signal is used to detect the private messages $\hat{W}_{p,k}$. Finally, the estimated message for user- k , \hat{W}_k , is obtained by combining $\hat{W}_{c,k}$ and $\hat{W}_{p,k}$. We note here that SDMA or conventional multiuser linear precoding is a subscheme of (1) that is obtained when we do not allocate any power to the common stream s_c and encode W_k into s_k . Hence, the sequel also holds for SDMA by simply turning off the common stream [21]–[24].

B. Quantization Model

We consider a linear model approximation for the quantization noise of the DACs, as also discussed in [32]. We define the uniform scalar quantizer function $Q(x)$ for a RF chain as

$$Q(u) \approx \delta u + \epsilon, \quad (3)$$

where the parameter δ represents the quantization resolution of b bits and is expressed in terms of b as

$$\delta = \sqrt{1 - \frac{\pi\sqrt{3}}{2} 2^{-2b}}. \quad (4)$$

The quantization noise $\epsilon \sim \mathcal{CN}(0, \sigma_\epsilon^2)$ and the input signal u are independent. The quantization noise variance is expressed

as $\sigma_e = \delta^2(1 - \delta^2)^2$. We assume that each RF chain has identical number of quantization bits. Substituting (1), the quantized transmitted signal \mathbf{x} is written as

$$Q(\mathbf{x}) \approx \mathbf{\Delta}\mathbf{x} + \boldsymbol{\epsilon}, \quad (5)$$

where $\mathbf{\Delta} = \text{Diag}(\delta_1, \delta_2, \dots, \delta_{N_t})$, $\boldsymbol{\epsilon} \sim \mathcal{CN}(\mathbf{0}_{N_t}, \boldsymbol{\Sigma})$ with $\boldsymbol{\Sigma} = \text{Diag}(\sigma_{e,1}, \sigma_{e,2}, \dots, \sigma_{e,N_t})$ and $\boldsymbol{\epsilon}$ is independent of \mathbf{x} . The power consumption of each active DAC is proportional to the number of quantization bits with the power consumption model expressed as

$$P(\delta) = \left[P_{\text{DAC}} \sqrt{\frac{\pi\sqrt{3}}{2(1-\delta^2)}} \right], \quad (6)$$

with P_{DAC} being the power consumption coefficient.

C. RSMA with DACs and RF Chain Selection for DFRC

We define the RF chain selection indicator $\lambda_i \in \{0, 1\}$ to represent the decision to activate the i -th RF-chain, such that, $\lambda_i = 1$ means the i -th RF-chain (and respectively the i -th antenna) is active. We further define the indicator vector and matrix as $\boldsymbol{\lambda} = [\lambda_1, \lambda_2, \dots, \lambda_{N_t}]$ and $\mathbf{\Lambda} = \text{Diag}[\lambda_1, \lambda_2, \dots, \lambda_{N_t}]$, respectively.

We consider a transmission model where L consecutive symbols are transmitted, with the symbol indexes chosen from the set $\mathcal{L} = \{1, 2, \dots, L\}$. We can express the l -th transmitted symbol for RSMA with RF chain selection under the quantization effects of the DACs from (1) and (5) as

$$\begin{aligned} \tilde{\mathbf{x}}_l &= Q(\mathbf{\Lambda}\mathbf{x}_l) = \mathbf{\Delta}(\mathbf{\Lambda}\mathbf{p}_{c,l} + \sum_{k=1}^K \mathbf{\Lambda}\mathbf{p}_{k,l}) + \boldsymbol{\Lambda}\boldsymbol{\epsilon}_l \\ &= \mathbf{\Delta}\mathbf{\Lambda}\mathbf{P}_l\mathbf{s}_l + \boldsymbol{\Lambda}\boldsymbol{\epsilon}_l, \quad \forall l \in \mathcal{L}. \end{aligned} \quad (7)$$

Using (2) and (7), the l -th received RSMA symbol at the user- k under DAC quantization error is written as

$$\tilde{\mathbf{y}}_{k,l}^c = \mathbf{h}_k^H \tilde{\mathbf{x}}_l + z_{k,l} = \mathbf{h}_k^H \mathbf{\Delta}\mathbf{\Lambda}\mathbf{P}_l\mathbf{s}_l + \underbrace{\mathbf{h}_k^H \boldsymbol{\Lambda}\boldsymbol{\epsilon}_l}_{\eta_{k,l}} + z_{k,l}, \quad (8)$$

where $\eta_{k,l} \sim \mathcal{CN}(0, \sigma_{\eta,k,l}^2)$, $\sigma_{\eta,k,l}^2 = \mathbf{h}_k^H \mathbf{\Lambda}\boldsymbol{\Sigma}\mathbf{\Lambda}\mathbf{h}_k + \sigma_n^2$ and the channel \mathbf{h}_k , $k \in \mathcal{K}$, is assumed to be static for L consecutive symbols. As it can be observed from the expression (8), the effects of DAC quantization is reflected by a multiplicative factor $\mathbf{\Delta}$ on the precoders and an increased noise variance.

We express the received Signal-to-Interference-Plus-Noise Ratios (SNRs) for the common and private streams at the l -th symbol and user- k as

$$\begin{aligned} \gamma_{c,k,l}(\mathbf{P}_l, \mathbf{\Lambda}, \mathbf{B}) &= \frac{|\mathbf{h}_k^H \mathbf{\Delta}\mathbf{\Lambda}\mathbf{p}_{c,l}|^2}{\sigma_n^2 + \mathbf{h}_k^H \mathbf{\Lambda}\boldsymbol{\Sigma}\mathbf{\Lambda}\mathbf{h}_k + \sum_{k' \in \mathcal{K}} |\mathbf{h}_k^H \mathbf{\Delta}\mathbf{\Lambda}\mathbf{p}_{k',l}|^2}, \\ \gamma_{k,l}(\mathbf{P}_l, \mathbf{\Lambda}, \mathbf{B}) &= \frac{|\mathbf{h}_k^H \mathbf{\Delta}\mathbf{\Lambda}\mathbf{p}_{k,l}|^2}{\sigma_n^2 + \mathbf{h}_k^H \mathbf{\Lambda}\boldsymbol{\Sigma}\mathbf{\Lambda}\mathbf{h}_k + \sum_{\substack{k' \in \mathcal{K}, \\ k' \neq k}} |\mathbf{h}_k^H \mathbf{\Delta}\mathbf{\Lambda}\mathbf{p}_{k',l}|^2}, \end{aligned}$$

where the matrix $\mathbf{B} = \text{Diag}[b_1, b_2, \dots, b_{N_t}]$ is used to represent the dependency on the number of quantization bits at each RF

chain. The rates of the common and private streams are written in terms of the SINR expressions as given below.

$$R_{c,k,l}(\mathbf{P}_l, \mathbf{\Lambda}, \mathbf{B}) = \log(1 + \gamma_{c,k,l}(\mathbf{P}_l, \mathbf{\Lambda}, \mathbf{B})), \quad (9)$$

$$R_{k,l}(\mathbf{P}_l, \mathbf{\Lambda}, \mathbf{B}) = \log(1 + \gamma_{k,l}(\mathbf{P}_l, \mathbf{\Lambda}, \mathbf{B})). \quad (10)$$

According to the RSMA framework, the common stream should be decodable by all receivers. Consequently, the rate of the common stream, denoted by $C_l(\mathbf{P}_l, \mathbf{\Lambda}, \mathbf{B})$, should be at most the minimum of the $R_{c,k,l}(\mathbf{P}_l, \mathbf{\Lambda}, \mathbf{B})$, $\forall k \in \mathcal{K}$, i.e.,

$$C_l(\mathbf{P}_l, \mathbf{\Lambda}, \mathbf{B}) = \min_{k \in \mathcal{K}} R_{c,k,l}(\mathbf{P}_l, \mathbf{\Lambda}, \mathbf{B}). \quad (11)$$

The transmit power is subject to the uniform elemental power constraint, which ensures that the power amplifiers driving the antenna elements are operated at full power at all times [40]. Accordingly, we write

$$\text{tr}(\mathbf{E}_i \mathbf{\Delta}\mathbf{P}_l \mathbf{s}_l \mathbf{s}_l^H \mathbf{P}_l^H \mathbf{\Delta}) = P_{ant}, \quad (12)$$

$\forall i \in \{1, 2, \dots, N_t\}$ and $\forall l \in \mathcal{L}$, where P_{ant} is the signal transmit power at each transmit antenna and \mathbf{E}_i is a diagonal matrix with the i -th diagonal element as 1 and the rest as 0.

D. Performance Metrics

In this section, we explain the metrics to be used in the constraints and objective function of the optimization problem that will be formulated to design the system.

1) Performance Metric for Communications

The communications performance of the system is measured in terms of the sum-rate, which is defined as

$$R_{sum}(\mathbf{P}, \mathbf{\Lambda}, \mathbf{B}) = \frac{1}{L} \sum_{l \in \mathcal{L}} \left(C_l(\mathbf{P}_l, \mathbf{\Lambda}, \mathbf{B}) + \sum_{k=1}^K R_{k,l}(\mathbf{P}_l, \mathbf{\Lambda}, \mathbf{B}) \right),$$

where $\mathbf{P} = [\mathbf{P}_1, \mathbf{P}_2, \dots, \mathbf{P}_L]$.

2) Performance Metric for Radar

In this work, we consider a co-located system and a point target model. Such a model is valid especially for detecting targets by means of co-located radars when the target distance is large compared to inter-element distance of the radar antenna array [41], [42].

Define the covariance matrix of the transmitted radar signal \mathbf{x}_l with L samples as

$$\mathbf{R}_x = \sum_{l \in \mathcal{L}} \mathbf{x}_l \mathbf{x}_l^H. \quad (13)$$

The covariance matrix of the transmitted signal can be used to investigate the detection probability [42] or angle/distance estimation performance for the radar. For each of the mentioned performance metrics, waveform designs with specific covariance matrix properties are known to achieve an optimal performance in terms of the metric in consideration. Therefore, we aim to design waveforms with covariance matrix properties similar to those of such radar-specific designs. Consequently, our radar performance metric is expressed as

$$\|\mathbf{R}_{\tilde{\mathbf{x}}}(\mathbf{P}, \mathbf{\Lambda}, \mathbf{B}) - \mathbf{U}\|_2 \leq \tau, \quad (14)$$

where \mathbf{U} represents the desired radar-signal covariance matrix and τ is the similarity threshold to the radar waveform.

In Section III-E, we provide more details on the considered radar performance metrics and the covariance matrix properties for the quantized RSMA joint communications and radar signal to achieve the optimal performance in terms of the considered metrics.

3) Performance Metric for the Objective Function

We consider the minimization of the EE metric for the objective function, which is defined as

$$\mathcal{E}(\mathbf{P}, \mathbf{\Lambda}, \mathbf{B}) = \frac{R_{sum}(\mathbf{P}_l, \mathbf{\Lambda}, \mathbf{B})}{P_{tot}(\mathbf{\Lambda}, \mathbf{B})}. \quad (15)$$

We express the total power consumption as [43]–[45]

$$P_{tot}(\mathbf{\Lambda}, \mathbf{B}) = \frac{\text{tr}(\mathbf{\Lambda})P_{ant}}{\eta_{PA}} + P_{RF} + \text{tr}(\mathbf{\Lambda}\mathbf{P}\mathbf{\Delta}) + P_{int} + P_{BB},$$

where $0 \leq \eta_{PA} \leq 1$ is the power amplifier efficiency, $\mathbf{P}\mathbf{\Delta} = \text{Diag}[P(\delta_1), P(\delta_2), \dots, P(\delta_{N_t})]$ and P_{BB} is the power consumption for baseband signal processing. The power consumption terms $P_{RF} = \text{tr}(\mathbf{\Lambda})P_{circ} + P_{syn}$ represents power consumption by analog hardware components with P_{circ} being the power consumed by analog circuitry in each RF chain and P_{syn} is the power consumed by frequency synthesizer. The term $P_{int} = p_{int}2S_{DAC}\text{tr}(\mathbf{\Lambda}\mathbf{B})$ represents the power consumed by data interface of the Digital Signal Processor (DSP) for each RF chain, where p_{int} is the power consumption per Gbps and S_{DAC} represents the sampling rate per port (I-Q) in Gbps [43].

III. PROBLEM FORMULATION AND PROPOSED ALGORITHMS

In this section, we formulate an EE maximization problem for joint radar and communications waveform design with RSMA and propose an algorithm to solve of the resulting formulation. Our aim is to determine the optimal number of quantization bits and the active RF chains to maximize EE under a radar performance metric.

A. Problem Formulation

We formulate the RSMA EE maximization problem for joint radar and communications for a given \mathbf{B} (and $\mathbf{\Delta}$ and $\mathbf{\Sigma}$) as

$$\max_{\mathbf{C}, \mathbf{P}, \mathbf{\Lambda}} \mathcal{E}(\mathbf{P}, \mathbf{\Lambda}, \mathbf{B}) \quad (16a)$$

$$\text{s.t. } C_l(\mathbf{P}_l, \mathbf{\Lambda}, \mathbf{B}) \leq R_{c,k,l}(\mathbf{P}_l, \mathbf{\Lambda}, \mathbf{B}), \quad (16b)$$

$$k \in \mathcal{K}, \forall l \in \mathcal{L} \quad (16c)$$

$$\lambda_i \in \{0, 1\}, i \in \{1, 2, \dots, N_t\}, \forall l \in \mathcal{L} \quad (16d)$$

$$\|\mathbf{R}_{\bar{\mathbf{x}}}(\mathbf{P}, \mathbf{\Lambda}, \mathbf{B}) - \mathbf{U}\|_2^2 \leq \tau \quad (16e)$$

$$R_{sum}(\mathbf{P}, \mathbf{\Lambda}, \mathbf{B}) \geq R_{th} \quad (16f)$$

$$\text{tr}(\mathbf{E}_i \mathbf{\Delta} \mathbf{P}_l \mathbf{s}_l \mathbf{s}_l^H \mathbf{P}_l^H \mathbf{\Delta}) = P_{ant}, \quad (16g)$$

$$i \in \{1, 2, \dots, N_t\}, \forall l \in \mathcal{L},$$

where $\mathbf{C} = [C_1, C_2, \dots, C_L]$, and R_{th} is the lower bound for the sum-rate. The constraint (16c) ensures the decodability of the common stream by all receivers, in accordance with the RSMA framework as described in Section II. The radar detection performance is controlled by subjecting the radar metric to the upper bound in the constraint (16e). A minimum

Algorithm 1: ADMM-Based Algorithm

```

t ← 0, v_r^0, u_r^0, w_r^0, ω, g, Λ, B
while ∑_{l∈L} ||r_{r,l}^t|| > ε_a or ∑_{l∈L} ||q_{r,l}^t|| > ε_a do
    v_r^{t+1} ← arg min_{v_r} (f(v_r, Λ, ω, g) +
    ½ ∑_{l∈L} ||v_{r,l} - u_{r,l}^t + w_{r,l}^t||^2) via interior-point
    methods
    u_r^{t+1} ←
    arg min_{u_r} (Π(u_r) + ½ ∑_{l∈L} ||v_{r,l}^{t+1} - u_{r,l} + w_{r,l}^t||^2)
    via SDR method
    w_{r,l}^{t+1} = w_{r,l}^t + v_{r,l}^{t+1} - u_{r,l}^{t+1}, ∀ l ∈ L
    r_{r,l}^{t+1} ← v_{r,l}^{t+1} - u_{r,l}^{t+1}, ∀ l ∈ L
    q_{r,l}^{t+1} ← u_{r,l}^{t+1} - u_{r,l}^t, ∀ l ∈ L
    t ← t + 1
end
return u_r^t

```

sum-rate performance is guaranteed by the constraint (16f). The constraint (16g) is the uniform elemental power constraint as discussed in Section II-C.

From the quantized signal model in (8), one can notice the transmit signal is a stochastic process due to the random quantization noise term ϵ . Proposition 1 gives an approximate form for the spatial covariance matrix of the quantized signal.

Proposition 1: For large L , the matrix $\mathbf{R}_{\bar{\mathbf{x}}}(\mathbf{P}, \mathbf{\Lambda}, \mathbf{B})$ can be approximately expressed as

$$\mathbf{R}_{\bar{\mathbf{x}}}(\mathbf{P}, \mathbf{\Lambda}, \mathbf{B}) \approx \sum_{l \in \mathcal{L}} \mathbf{\Delta} \mathbf{\Lambda} \mathbf{P}_l \mathbf{s}_l \mathbf{s}_l^H \mathbf{P}_l^H \mathbf{\Lambda} \mathbf{\Delta} + L \mathbf{\Lambda} \mathbf{\Sigma} \mathbf{\Lambda}. \quad (17)$$

$$\triangleq \bar{\mathbf{R}}_{\bar{\mathbf{x}}}(\mathbf{P}, \mathbf{\Lambda}, \mathbf{B}).$$

Proof: Please see Appendix VII-A. ■

The problem formulation (16) is not convex with respect to the optimization parameters \mathbf{P} and $\mathbf{\Lambda}$, and is challenging to solve. In the following sections, we describe our proposed AO-based algorithm that alternates between finding the optimal precoders for given RF chain selection matrix and finding optimal RF chain selection matrix for given precoders by solving separate subproblems. The subproblem of finding the optimal precoders is solved by an ADMM-based algorithm and the problem of finding optimal RF chain selection matrix for given precoders is solved by an SCA/SDR-based algorithm.

B. Proposed AO-ADMM Based Algorithm for Optimal Precoder Calculation

We define $\mathbf{v} = [\mathbf{v}_1^T, \mathbf{v}_2^T, \dots, \mathbf{v}_L^T]^T$, $\mathbf{v}_l = [C_l, \text{vec}(\mathbf{P}_l)^T]^T$, and $f(\mathbf{v}) = \mathcal{E}(\mathbf{v}, \mathbf{\Lambda}, \mathbf{B})$. We reformulate the problem (16) according to the ADMM framework [46] as

$$\min_{\mathbf{v}, \mathbf{u}} -f(\mathbf{v}) + \Pi(\mathbf{u}) \quad (18a)$$

$$\text{s.t. } \mathbf{v} - \mathbf{u} = \mathbf{0}, \quad (18b)$$

where $\mathbf{u}_l, \forall l \in \mathcal{L}$ and $\mathbf{u} = [\mathbf{u}_1^T, \mathbf{u}_2^T, \dots, \mathbf{u}_L^T]^T$ are introduced to split the problem according to the ADMM procedure.

The function $\Pi(\mathbf{v})$ is the indicator function that performs projection on the domain \mathcal{D} defined by the constraints (16c), (16e) and (16g), i.e., $\Pi(\mathbf{u}) = 0$ if $\mathbf{u} \in \mathcal{D}$ and $\Pi(\mathbf{u}) = \infty$ if $\mathbf{u} \notin \mathcal{D}$. We also define the real-valued

vectors $\mathbf{v}_{r,l} = [\Re(\mathbf{v}_l^T), \Im(\mathbf{v}_l^T)]^T$, $\mathbf{u}_{r,l} = [\Re(\mathbf{u}_l^T), \Im(\mathbf{u}_l^T)]^T$, $\mathbf{v}_r = [\mathbf{v}_{r,1}^T, \mathbf{v}_{r,2}^T \dots, \mathbf{v}_{r,L}^T]^T$ and $\mathbf{u}_r = [\mathbf{u}_{r,1}^T, \mathbf{u}_{r,2}^T \dots, \mathbf{u}_{r,L}^T]^T$ in accordance with the ADMM framework, where the functions $\Re(\cdot)$ and $\Im(\cdot)$ return the real and imaginary parts of their inputs, respectively.

The augmented Lagrangian function for the optimization problem (18) is written as

$$\mathcal{L}_\zeta(\mathbf{v}_r, \mathbf{u}_r, \mathbf{d}_r) = -f(\mathbf{v}_r) + \Pi(\mathbf{u}_r) + \sum_{l \in \mathcal{L}} \mathbf{d}_{r,l}^T (\mathbf{v}_{r,l} - \mathbf{u}_{r,l}) + \sum_{l \in \mathcal{L}} (\zeta/2) \|\mathbf{v}_{r,l} - \mathbf{u}_{r,l}\|_2^2,$$

where $\zeta > 0$ is called the penalty parameter, $\mathbf{d}_r = [\mathbf{d}_{r,1}^T, \mathbf{d}_{r,2}^T \dots, \mathbf{d}_{r,L}^T]^T$ and $\mathbf{d}_{r,n} = [\Re(\mathbf{d}_n^T), \Im(\mathbf{d}_n^T)]^T$ and $\mathbf{d}_l \in \mathbb{C}^{(1+N_t)(K+1)}$, $\forall l \in \mathcal{L}$ being the dual variables.

The updates of iterative ADMM procedure can be written in the scaled form as

$$\mathbf{v}_r^{t+1} = \arg \min_{\mathbf{v}_r} (-f(\mathbf{v}_r) + \frac{\zeta}{2} \sum_{l \in \mathcal{L}} \|\mathbf{v}_{r,l} - \mathbf{u}_{r,l}^t + \mathbf{w}_{r,l}^t\|_2^2) \quad (19)$$

$$\mathbf{u}_r^{t+1} = \arg \min_{\mathbf{u}_r} (\Pi(\mathbf{u}_r) + \frac{\zeta}{2} \sum_{l \in \mathcal{L}} \|\mathbf{v}_{r,l}^{t+1} - \mathbf{u}_{r,l} + \mathbf{w}_{r,l}^t\|_2^2) \quad (20)$$

$$\mathbf{w}_{r,n}^{t+1} = \mathbf{w}_{r,l}^t + \mathbf{v}_{r,l}^{t+1} - \mathbf{u}_{r,l}^{t+1}, \quad \forall l \in \mathcal{L}, \quad (21)$$

where $\mathbf{w}_r = \mathbf{d}_r / \zeta$. The update step for \mathbf{v}_r in (19) deals with the WMSE minimization problem. The update step for \mathbf{u}_r in (20) involves projection onto the domain \mathcal{D} .

We note that for given \mathbf{B} and \mathbf{A} , the objective function $f(\mathbf{v})$ and the constraint (16c) are not convex with respect to \mathbf{v} . Rate-Mean Square Error (MSE) transformations are used in [23] to transform the non-convex sum-rate function for RSMA into a convex one. We first obtain the optimal receive filter, $g_{k,l}$, that minimizes the MSE $\mathbb{E}\{|\epsilon_{k,l}|^2\} = \mathbb{E}\{|g_{k,l} y_{k,l} - x_{k,l}|^2\}$, $\forall k \in \mathcal{K}$, $\forall l \in \mathcal{L}$. It is well known that the solution is given by a Minimum MSE (MMSE) filter

$$g_{k,l}^{\text{opt}} = \frac{\mathbf{p}_{k,l}^H \mathbf{A} \Delta \mathbf{h}_k}{\sigma_n^2 + \mathbf{h}_k^H \mathbf{A} \Sigma \mathbf{A} \mathbf{h}_k + \sum_{k' \in \mathcal{K}} |\mathbf{h}_k^H \Delta \mathbf{A} \mathbf{p}_{k',l}|^2},$$

$$g_{c,k,l}^{\text{opt}} = \frac{\mathbf{p}_{c,k,l}^H \mathbf{A} \Delta \mathbf{h}_k}{\sigma_n^2 + \mathbf{h}_k^H \mathbf{A} \Sigma \mathbf{A} \mathbf{h}_k + \sum_{k' \in \{c, \mathcal{K}\}} |\mathbf{h}_k^H \Delta \mathbf{A} \mathbf{p}_{k',l}|^2}. \quad (22)$$

The resulting MSE is written as

$$\epsilon_{k,l}^{\text{opt}} = \frac{\sigma_n^2 + \mathbf{h}_k^H \mathbf{A} \Sigma \mathbf{A} \mathbf{h}_k + \sum_{\substack{k' \in \mathcal{K} \\ k' \neq k}} |\mathbf{h}_k^H \Delta \mathbf{A} \mathbf{p}_{k',l}|^2}{\sigma_n^2 + \mathbf{h}_k^H \mathbf{A} \Sigma \mathbf{A} \mathbf{h}_k + \sum_{k' \in \mathcal{K}} |\mathbf{h}_k^H \Delta \mathbf{A} \mathbf{p}_{k',l}|^2},$$

$$\epsilon_{c,k,l}^{\text{opt}} = \frac{\sigma_n^2 + \mathbf{h}_k^H \mathbf{A} \Sigma \mathbf{A} \mathbf{h}_k + \sum_{k' \in \mathcal{K}} |\mathbf{h}_k^H \Delta \mathbf{A} \mathbf{p}_{k',l}|^2}{\sigma_n^2 + \mathbf{h}_k^H \mathbf{A} \Sigma \mathbf{A} \mathbf{h}_k + \sum_{k' \in \{c, \mathcal{K}\}} |\mathbf{h}_k^H \Delta \mathbf{A} \mathbf{p}_{k',l}|^2}. \quad (23)$$

Following the approach in [23], we define the augmented weighted MSEs (WMSEs) as

$$\xi_{c,k,l} = \omega_{c,k,l} \epsilon_{c,k,l} - \log_2(\omega_{c,k,l}),$$

$$\xi_{k,l} = \omega_{k,l} \epsilon_{k,l} - \log_2(\omega_{k,l}), \quad (24)$$

where $\omega_{c,k,l}$ and $\omega_{k,l}$ are the weights for the MSEs of the common and private streams at user- k and symbol- l . It can be shown that the optimum weights are given by $\omega_{c,k,l}^{\text{opt}} = (\epsilon_{c,k,l}^{\text{opt}})^{-1}$ and $\omega_{k,l}^{\text{opt}} = (\epsilon_{k,l}^{\text{opt}})^{-1}$, for which the MSE-mutual information relations are obtained as $\xi_{k,l}^{\text{opt}} = 1 - R_{k,l}$

Algorithm 2: AO-ADMM-Based Algorithm

```

 $t \leftarrow 0, \mathbf{v}_r^0, \mathbf{u}_r^0, \mathbf{w}_r^0, \mathbf{A}, \mathbf{B}$ 
while  $|\mathbb{E}E^t - \mathbb{E}E^{t-1}| > \epsilon_r$  do
   $\boldsymbol{\omega}^t \leftarrow \text{updateWeights}(\mathbf{u}_r^t, \mathbf{A})$ 
   $\mathbf{g}^t \leftarrow \text{updateFilters}(\mathbf{u}_r^t, \mathbf{A})$ 
   $[\mathbf{u}_r^{t+1}, \mathbf{w}_r^{t+1}] \leftarrow \mathbf{ALG1}(b, \mathbf{A}, \mathbf{u}_r^t, \mathbf{w}_r^t, \boldsymbol{\omega}^t, \mathbf{g}^t)$ 
   $\mathbb{E}E^{t+1} \leftarrow \text{updateEE}(\mathbf{u}_r^{t+1})$ 
   $t \leftarrow t + 1$ 
end
return  $\mathbf{u}_r^t$ 

```

and $\xi_{c,k,l}^{\text{opt}} = 1 - R_{c,k,l}$. Accordingly, the average augmented MSE-rate transformations are written as

$$\xi_{c,k,l}^{\text{opt}} = 1 - R_{c,k,l}, \quad \xi_{k,l}^{\text{opt}} = 1 - R_{k,l}, \quad \forall l \in \mathcal{L}. \quad (25)$$

For given \mathbf{A} , $\boldsymbol{\omega}_l = [\omega_{c,1,l}, \omega_{1,l} \dots, \omega_{c,K,l}, \omega_{K,l}]^T$, $\boldsymbol{\omega} = [\boldsymbol{\omega}_1^T, \dots, \boldsymbol{\omega}_L^T]^T$, $\mathbf{g} = [g_{c,1,l}, g_{1,l} \dots, g_{c,K,l}, g_{K,l}]^T$ and $\mathbf{g} = [\mathbf{g}_1^T, \dots, \mathbf{g}_L^T]^T$, it is straightforward to show that maximizing $f(\mathbf{v}) = \mathcal{E}(\mathbf{v}, \mathbf{A}, \mathbf{B})$ is equivalent to minimizing $\bar{f}(\mathbf{v}) = \frac{1}{L} \sum_{l \in \mathcal{L}} (\xi_{c,l} + \sum_{k \in \mathcal{K}} \xi_{k,l})$, and $\bar{f}(\mathbf{v})$ is a convex function of \mathbf{v} (for given \mathbf{A} , $\boldsymbol{\omega}$ and \mathbf{g}). Then, the update operation in (19) is rewritten in terms of $\bar{f}(\mathbf{v}_r)$ as

$$\mathbf{v}_r^{t+1} = \arg \min_{\mathbf{v}_r} (\bar{f}(\mathbf{v}_r) + \frac{\zeta}{2} \sum_{l \in \mathcal{L}} \|\mathbf{v}_{r,l} - \mathbf{u}_{r,l}^t + \mathbf{w}_{r,l}^t\|_2^2) \quad (26)$$

Similarly, the constraint (16c) is written in terms of augmented MSEs as

$$\bar{\xi}_{c,l} \geq \bar{\xi}_{c,k,l}, \quad \forall k \in \mathcal{K}, \quad \forall l \in \mathcal{L}. \quad (27)$$

The ADMM-based algorithm to perform the updates in (20), (26) for given $\boldsymbol{\omega}$ and \mathbf{g} is described in Alg. 1. The update step for \mathbf{v}_r can be solved using interior-point methods as described in [23]¹. We propose the SDR method for the update step for \mathbf{u}_r to deal with the non-convex constraint (16g) [47]. Consider the following formulation for the minimization step for \mathbf{u} expressed in terms of the complex-valued parameters as

$$\min_{\mathbf{u}} \sum_{l \in \mathcal{L}} \|\mathbf{v}_l^{t+1} - \mathbf{u}_l + \mathbf{w}_l^t\|_2^2 \quad (28a)$$

$$\text{s.t. } \mathbf{e}_1^T \mathbf{u}_l \geq \xi_{c,k,l}, \quad \forall k \in \mathcal{K}, \quad \forall l \in \mathcal{L} \quad (28b)$$

$$\|\bar{\mathbf{R}}_{\bar{\mathbf{x}}}(\mathbf{u}, \mathbf{A}, \mathbf{B}) - \mathbf{U}\|_2^2 \leq \tau \quad (28c)$$

$$R_{\text{sum}}(\mathbf{u}, \mathbf{A}, \mathbf{B}) \geq R_{\text{th}} \quad (28d)$$

$$\text{tr}(\mathbf{E}_i(\boldsymbol{\Theta} \mathbf{u}_l)(\boldsymbol{\Theta} \mathbf{u}_l)^H) = P_{\text{ant}},$$

$$i \in \{1, 2, \dots, N_t\}, \quad \forall l \in \mathcal{L}. \quad (28e)$$

¹We note that the work in [23] deals with a purely communications problem and does not employ an ADMM-based algorithm. However, inserting the ADMM penalty term $\frac{\zeta}{2} \sum_{l \in \mathcal{L}} \|\mathbf{v}_{r,l} - \mathbf{u}_{r,l}^t + \mathbf{w}_{r,l}^t\|_2^2$ and the radar metric constraint (16e) to the applied solution is a straightforward task.

where

$$\begin{aligned}\bar{\mathbf{R}}_{\bar{\mathbf{x}}}(\mathbf{u}, \bar{\mathbf{\Lambda}}, \mathbf{B}) &= \sum_{l \in \mathcal{L}} \Theta \mathbf{S}_l \bar{\Delta} \bar{\mathbf{\Lambda}} \mathbf{u}_l \mathbf{u}_l^H \bar{\mathbf{\Lambda}} \bar{\Delta} \mathbf{S}_l^H \Theta^H + L \mathbf{\Lambda} \Sigma \mathbf{\Lambda} \\ \mathbf{S}_l &= \text{Diag}([0, \underbrace{s_{c,l}, \dots, s_{c,l}}_{N_t}, \underbrace{s_{1,l}, \dots, s_{1,l}}_{N_t}, \dots, \underbrace{s_{K,l}, \dots, s_{K,l}}_{N_t}]) \\ \bar{\mathbf{\Lambda}} &= \text{Diag}([0, \underbrace{\lambda_1, \lambda_2, \dots, \lambda_{N_t}, \dots, \lambda_1, \lambda_2, \dots, \lambda_{N_t}}_{(K+1)N_t}]) \\ \bar{\Delta} &= \text{Diag}([0, \underbrace{\delta_1, \delta_2, \dots, \delta_{N_t}, \dots, \delta_1, \delta_2, \dots, \delta_{N_t}}_{(K+1)N_t}]) \\ \Theta &= ([\mathbf{0}^{N_t \times 1}, \underbrace{\mathbf{I}_{N_t}, \dots, \mathbf{I}_{N_t}}_{K+1}]),\end{aligned}$$

and \mathbf{e}_k is the k -th standard basis vector of length $N_t(K+1)+1$. The inhomogeneous Quadratically Constrained Quadratic Program (QCQP) formulation (28) can be transformed into an equivalent homogeneous QCQP as demonstrated in [47], and the resulting problem can be solved by applying the SDR procedure. We omit the rest of the details on the application of the SDR procedure due to lack of space and refer the interested reader to [47].

Alg. 2 describes the AO-ADMM-based algorithm to solve the updates in (19)-(21) using the ADMM-based in Alg. 1 and $\boldsymbol{\omega}$ and \mathbf{g} calculations. The outer iterations of the AO algorithm serve to update the MSE weights $\boldsymbol{\omega}^i$ and equalizers \mathbf{g}^i based on the precoders calculated by the ADMM-based algorithm at iteration- i . By the calculated $\boldsymbol{\omega}^i$ and \mathbf{g}^i , the ADMM algorithm performs the update steps in (19) and (20).

Proposition 2: For given $\mathbf{\Lambda}$, the proposed algorithm in Alg. (2) converges to a stationary point of the problem (16).

Proof: We prove the convergence of the proposed AO-ADMM-based algorithm in Alg. (2) over the real-valued equivalent definitions of the functions. First, consider the inner problem in Alg. (2) solved by the ADMM-based algorithm in Alg. (1),

$$\begin{aligned}\min_{\mathbf{v}_r} \quad & \bar{f}(\mathbf{v}_r, \mathbf{\Lambda}, \boldsymbol{\omega}^i, \mathbf{g}^i) \\ \text{s.t.} \quad & \mathbf{v}_r \in \mathcal{D}^i,\end{aligned}$$

where \mathcal{D}^i represents the problem domain in the i -th iteration of the AO algorithm. It can be shown that the function $\bar{f}(\mathbf{v}_r, \mathbf{\Lambda}, \boldsymbol{\omega}^i, \mathbf{g}^i)$ is Lipschitz differentiable [48] and \mathcal{D}^i is a compact set. Then, the sequence $(\mathbf{v}_r^t, \mathbf{u}_r^t, \mathbf{w}_r^t)$ has at least one limit point, and each limit point is a stationary point of $\mathcal{L}_\zeta(\mathbf{v}_r, \mathbf{u}_r, \mathbf{w}_r)$ for any sufficiently large ζ [48, Cor. 2]. This is also valid when the subproblems are solved inexactly with summable errors, which is a condition satisfied by the SDR method [49].

Since the solution \mathbf{u}_r^t at iteration t is also a feasible solution at iteration $t+1$, the EE^t is non-decreasing with t and is bounded above due to the per antenna power constraints, per antenna RF chain power consumption and the constant terms P_{BB} and P_{syn} in $\mathcal{E}(\mathbf{P}, \mathbf{\Lambda}, \mathbf{B})$ [45] [50, Sec. IV-F] [51]. Given the convergence of the ADMM part for the inner iterations and EE^t being bounded, the convergence of the AO algorithm for the outer iterations follow from [23, Prop. 1]. ■

We note that due to the non-convex nature of the problem, the global optimality of the solutions cannot be guaranteed and is dependent on the initializations of the precoders.

C. Proposed SCA/SDR-Based Algorithm for Optimal RF Chain Selection

The sub-problem to find the optimal RF chain selection matrix for given precoders ($\mathbf{P}^{(t)}$ at iteration t) can be written as

$$\max_{\mathbf{C}, \mathbf{\Lambda}} \frac{\frac{1}{L} \sum_{l \in \mathcal{L}} (C_l(\mathbf{P}_l^{(t)}, \mathbf{\Lambda}, \mathbf{B}) + \sum_{k \in \mathcal{K}} R_{k,l}(\mathbf{P}_l^{(t)}, \mathbf{\Lambda}, \mathbf{B}))}{P_{tot}(\mathbf{\Lambda}, \mathbf{B})} \quad (30a)$$

$$\text{s.t.} \quad C_l(\mathbf{P}_l^{(t)}, \mathbf{\Lambda}, \mathbf{B}) \leq R_{c,k,l}(\mathbf{P}_l^{(t)}, \mathbf{\Lambda}, \mathbf{B}), \quad k \in \mathcal{K}, \forall l \in \mathcal{L} \quad (30b)$$

$$\lambda_i \in \{0, 1\}, \quad i \in \{1, 2, \dots, N_t\}, \quad \forall l \in \mathcal{L} \quad (30c)$$

$$\left\| \bar{\mathbf{R}}_{\bar{\mathbf{x}}}(\mathbf{P}^{(t)}, \mathbf{\Lambda}, \mathbf{B}) - \mathbf{U} \right\|_2^2 \leq \tau \quad (30d)$$

$$R_{sum}(\mathbf{P}^{(t)}, \mathbf{\Lambda}, \mathbf{B}) \geq R_{th}. \quad (30e)$$

The problem (30) is non-convex due to the non-convex objective function and the constraints (30b), (30d), and (30e) with respect to $\mathbf{\Lambda}$. Before moving to obtain a convex equivalent formulation for the considered problem, we introduce the following lemma.

Lemma 1: Define the vectors $\mathbf{a}, \mathbf{b}, \mathbf{c} \in \mathbb{C}^{M \times 1}$ and the matrix $\mathbf{D}_b = \text{Diag}(\mathbf{b}^T)$. Then, the following holds

$$\mathbf{a}^H \mathbf{D}_b \mathbf{c} = \mathbf{b}^T (\mathbf{a}^* \circ \mathbf{c}), \quad (31)$$

where \circ represents the Hadamard product.

Proof: We start by writing $\mathbf{a}^H \mathbf{D}_b \mathbf{c}$ by using the Hadamard product as

$$\mathbf{a}^H \mathbf{D}_b \mathbf{c} = \mathbf{a}^H (\mathbf{b} \circ \mathbf{c}). \quad (32)$$

Using the property $\mathbf{x}^H (\mathbf{X} \circ \mathbf{Y}) \mathbf{y} = \text{tr}(\mathbf{D}_x^H \mathbf{X} \mathbf{D}_y \mathbf{Y}^T)$, we write

$$\mathbf{a}^H (\mathbf{b} \circ \mathbf{c}) = \text{tr}(\mathbf{D}_a^H \mathbf{b} \mathbf{c}^T) = \mathbf{c}^T \mathbf{D}_a^H \mathbf{b} = \mathbf{b}^T \mathbf{D}_a^H \mathbf{c}.$$

Finally, using the property in (32) once again, we obtain

$$\mathbf{b}^T \mathbf{D}_a^H \mathbf{c} = \mathbf{b}^T (\mathbf{a}^* \circ \mathbf{c}), \quad (33)$$

which completes the proof. ■

We benefit from Lemma 1 to rewrite the rate expressions as given below.

$$\begin{aligned}R_{k,l}(\mathbf{P}_l, \mathbf{\Lambda}, \mathbf{B}) &= \log \left(1 + \frac{|\boldsymbol{\lambda}^T (\Delta \mathbf{h}_k^* \circ \mathbf{p}_{k,l})|^2}{\sigma_n^2 + \boldsymbol{\lambda}^T \Phi \boldsymbol{\lambda} + \sum_{k' \in \mathcal{K}, k' \neq k} |\boldsymbol{\lambda}^T (\Delta \mathbf{h}_k^* \circ \mathbf{p}_{k',l})|^2} \right), \quad (34)\end{aligned}$$

$$\begin{aligned}R_{c,k,l}(\mathbf{P}_l, \mathbf{\Lambda}, \mathbf{B}) &= \log \left(1 + \frac{|\boldsymbol{\lambda}^T (\Delta \mathbf{h}_k^* \circ \mathbf{p}_{c,l})|^2}{\sigma_n^2 + \boldsymbol{\lambda}^T \Phi \boldsymbol{\lambda} + \sum_{k' \in \mathcal{K}} |\boldsymbol{\lambda}^T (\Delta \mathbf{h}_k^* \circ \mathbf{p}_{k',l})|^2} \right), \quad (35)\end{aligned}$$

where $\Phi = \text{Diag}([\sigma_{e,1}^2 |h_{1,1}|^2, \sigma_{e,2}^2 |h_{2,1}|^2, \dots, \sigma_{e,N_t}^2 |h_{N_t,1}|^2])$ and

$$\max_{\mathbf{C}', \Lambda, t} t \quad (36a)$$

$$\text{s.t. } t \leq \frac{\frac{1}{L} \sum_{l \in \mathcal{L}} \left(C'_l + \sum_{k \in \mathcal{K}} \ln(\sigma_n^2 + \lambda^T \Phi \lambda + \sum_{k' \in \mathcal{K}} |\lambda^T (\Delta \mathbf{h}_k^* \circ \mathbf{p}_{k',l})|^2) - \ln(\sigma_n^2 + \lambda^T \Phi \lambda + \sum_{\substack{k' \in \mathcal{K}, \\ k' \neq k}} |\lambda^T (\Delta \mathbf{h}_k^* \circ \mathbf{p}_{k',l})|^2) \right)}{\ln 2(P_{\text{tot}}(\Lambda, \mathbf{B}))} \quad (36b)$$

$$C'_l \leq \ln \left(\sigma_n^2 + \lambda^T \Phi \lambda + \sum_{k' \in \{\mathcal{K}, c\}} |\lambda^T (\Delta \mathbf{h}_k^* \circ \mathbf{p}_{k',l})|^2 \right) - \ln \left(\sigma_n^2 + \lambda^T \Phi \lambda + \sum_{k' \in \mathcal{K}} |\lambda^T (\Delta \mathbf{h}_k^* \circ \mathbf{p}_{k',l})|^2 \right), \quad k \in \mathcal{K}, \forall l \in \mathcal{L} \quad (36c)$$

$$\frac{1}{L} \sum_{l \in \mathcal{L}} \left(C'_l + \sum_{k \in \mathcal{K}} \ln(\sigma_n^2 + \lambda^T \Phi \lambda + \sum_{k' \in \mathcal{K}} |\lambda^T (\Delta \mathbf{h}_k^* \circ \mathbf{p}_{k',l})|^2) - \ln(\sigma_n^2 + \lambda^T \Phi \lambda + \sum_{\substack{k' \in \mathcal{K}, \\ k' \neq k}} |\lambda^T (\Delta \mathbf{h}_k^* \circ \mathbf{p}_{k',l})|^2) \right) \geq \ln 2R_{\text{th}} \quad (36d)$$

(30c), (30d).

the second term in the denominator follows from the fact that $\mathbf{D}_a \mathbf{b} = \mathbf{D}_b \mathbf{a}$.

First, we write an equivalent problem as in (36), with $C'_l = \ln 2C_l$. Then, we introduce the slack variables $\omega_{k,l}$ and $\nu_{k,l}$ and rewrite the constraint (36c) in 3 new constraints as

$$\ln \left(\sigma_n^2 + \lambda^T \Phi \lambda + \sum_{k' \in \mathcal{K}} |\lambda^T (\Delta \mathbf{h}_k^* \circ \mathbf{p}_{k',l})|^2 \right) \leq \omega_{k,l}, \quad (37a)$$

$$\ln \left(\sigma_n^2 + \lambda^T \Phi \lambda + \sum_{k' \in \{\mathcal{K}, c\}} |\lambda^T (\Delta \mathbf{h}_k^* \circ \mathbf{p}_{k',l})|^2 \right) \geq \nu_{k,l}, \quad (37b)$$

$$C'_l - \nu_{k,l} + \omega_{k,l} \leq 0, \quad k \in \mathcal{K}, \forall l \in \mathcal{L}. \quad (37c)$$

Next, we simplify the expressions using a stacking method employed in [52], [53]. Define the matrices

$$\Gamma_k = \sigma_n^2 \mathbf{I}_{N_t} + \Phi + \sum_{k' \in \mathcal{K}} (\Delta \mathbf{h}_k^* \circ \mathbf{p}_{k',l}) (\Delta \mathbf{h}_k^* \circ \mathbf{p}_{k',l})^H,$$

$$\Xi_k = \frac{\sigma_n^2}{N_t} \mathbf{I}_{N_t} + \Phi + \sum_{k' \in \{\mathcal{K}, c\}} (\Delta \mathbf{h}_k^* \circ \mathbf{p}_{k',l}) (\Delta \mathbf{h}_k^* \circ \mathbf{p}_{k',l})^H.$$

Keeping in mind that $1 \leq \|\lambda\|^2 \leq N_t$, we can write

$$\sigma_n^2 + \lambda^T \Phi \lambda + \sum_{k' \in \mathcal{K}} |\lambda^T (\Delta \mathbf{h}_k^* \circ \mathbf{p}_{k',l})|^2 \leq \lambda^T \Gamma_k \lambda \leq e^{\omega_{k,l}} \quad (38)$$

$$\sigma_n^2 + \lambda^T \Phi \lambda + \sum_{k' \in \{\mathcal{K}, c\}} |\lambda^T (\Delta \mathbf{h}_k^* \circ \mathbf{p}_{k',l})|^2 \geq \lambda^T \Xi_k \lambda \geq e^{\nu_{k,l}} \quad (39)$$

One can observe that the constraints (38) and (39) are not convex. In order to obtain convex approximations of the considered constraints, we introduce the matrix $\Upsilon = \lambda \lambda^T$ into the expressions and apply first order Taylor approximation on (38) around the point $\omega_{k,l}^{t-1}$ to get

$$\text{tr}(\Upsilon \Gamma_k) \leq e^{\omega_{k,l}^{t-1}} (\omega_{k,l} - \omega_{k,l}^{t-1} + 1) \quad (40a)$$

$$\text{tr}(\Upsilon \Xi_k) \geq e^{\nu_{k,l}}. \quad (40b)$$

Algorithm 3: SCA/SDR-based algorithm

```

t ← 0, P, B
while |EEt - EEt-1| > εr do
  (Υ, C', αt+1, βt+1, γt+1, ωt+1, νt+1, κt+1) ←
  (48) for given αt, βt, γt, ωt via interior-point
  methods
  Λ ← updateInd(Υ)
  EEt+1 ← updateEE(Λ)
  t ← t + 1
end
return Λt

```

Next, we define the auxiliary variables α_l , β , $\kappa_{k,l}$ and $\gamma_{k,l}$ and write the constraint (36b) by means of 5 new constraints

$$t \leq \frac{\frac{1}{L} \sum_{l \in \mathcal{L}} \alpha_l^2}{\beta}, \quad (41a)$$

$$\ln \left(\sigma_n^2 + \lambda^T \Phi \lambda + \sum_{\substack{k' \in \mathcal{K}, \\ k' \neq k}} |\lambda^T (\Delta \mathbf{h}_k^* \circ \mathbf{p}_{k',l})|^2 \right) \leq \gamma_{k,l}, \quad (41b)$$

$$\ln \left(\sigma_n^2 + \lambda^T \Phi \lambda + \sum_{k' \in \mathcal{K}} |\lambda^T (\Delta \mathbf{h}_k^* \circ \mathbf{p}_{k',l})|^2 \right) \geq \kappa_{k,l}, \quad (41c)$$

$$\alpha_l^2 - C'_l - \sum_{k \in \mathcal{K}} \kappa_{k,l} + \sum_{k \in \mathcal{K}} \gamma_{k,l} \leq 0, \quad \forall l \in \mathcal{L} \quad (41d)$$

$$P_{\text{tot}}(\Lambda, \mathbf{B}) \leq \beta / \ln 2. \quad (41e)$$

Similar to the approach taken for (37), we first define the matrices

$$\Psi_k = \sigma_n^2 \mathbf{I}_{N_t} + \Phi + \sum_{\substack{k' \in \mathcal{K}, \\ k' \neq k}} (\Delta \mathbf{h}_k^* \circ \mathbf{p}_{k',l}) (\Delta \mathbf{h}_k^* \circ \mathbf{p}_{k',l})^H,$$

$$\Omega_k = \frac{\sigma_n^2}{N_t} \mathbf{I}_{N_t} + \Phi + \sum_{k' \in \{\mathcal{K}\}} (\Delta \mathbf{h}_k^* \circ \mathbf{p}_{k',l}) (\Delta \mathbf{h}_k^* \circ \mathbf{p}_{k',l})^H,$$

and apply first order Taylor approximations to obtain the convex approximations for the constraints (41a), (41b) and

(41c), respectively, as

$$t \leq \frac{1}{L} \sum_{l \in \mathcal{L}} \left(\frac{2\alpha_l^{t-1}}{\beta^{t-1}} \right) \alpha_l - \left(\frac{\alpha_l^{t-1}}{\beta^{t-1}} \right)^2 \beta. \quad (42a)$$

$$\text{tr}(\mathbf{Y}\Psi_k) \leq e^{\gamma_{k,l}^{t-1}} (\gamma_{k,l} - \gamma_{k,l}^{t-1} + 1), \quad (42b)$$

$$\text{tr}(\mathbf{Y}\Omega_k) \geq e^{\kappa_{k,l}}. \quad (42c)$$

Using $\lambda_i \in \{0, 1\}$, we can express the constraint (41e) in terms of \mathbf{Y} as

$$\begin{aligned} P_{tot}(\mathbf{Y}, \mathbf{B}) &= \frac{\text{tr}(\mathbf{Y})P_{ant}}{\eta_{PA}} + P_{RF} + \text{tr}(\mathbf{Y}\mathbf{P}\Delta) + P_{int} + P_{BB} \\ &\leq \beta / \ln 2, \end{aligned} \quad (43)$$

with $P_{RF} = \text{tr}(\mathbf{Y})P_{circ} + P_{syn}$ and $P_{int} = p_{int} 2S_{DAC} \text{tr}(\mathbf{Y}\mathbf{B})$.

For the constraint (36d), we use the auxiliary variables $\kappa_{k,l}$ and $\gamma_{k,l}$ to write

$$\frac{1}{L} \sum_{l \in \mathcal{L}} \left(C'_l + \sum_{k \in \mathcal{K}} \kappa_{k,l} - \sum_{k \in \mathcal{K}} \gamma_{k,l} \right) \geq \ln 2 R_{th}. \quad (44)$$

Next, we move to rewrite the constraint (30d) in terms of \mathbf{Y} . Proposition 3 gives the expression for $\bar{\mathbf{R}}_{\bar{\mathbf{x}}}(\mathbf{P}, \mathbf{A}, \mathbf{B})$ in terms of \mathbf{Y} .

Proposition 3: The matrix $\bar{\mathbf{R}}_{\bar{\mathbf{x}}}(\mathbf{P}, \mathbf{A}, \mathbf{B})$ can be expressed in terms of \mathbf{Y} as

$$\bar{\mathbf{R}}_{\bar{\mathbf{x}}}(\mathbf{P}, \mathbf{A}, \mathbf{B}) = \sum_{l \in \mathcal{L}} \sum_{i=1}^{N_t} (\mu_{i,l} \mathbf{F}_{i,l} \mathbf{Y} \mathbf{F}_{i,l}^H + \Sigma \mathbf{E}_i \mathbf{Y} \mathbf{E}_i), \quad (45)$$

where $\mathbf{F}_{i,l} = \text{Diag}(\mathbf{f}_{i,l})$ and $\mu_{i,l}$ and $\mathbf{f}_{i,l}$ are respectively the i -th eigenvalue and eigenvector of the matrix $\Delta \mathbf{P}_l \mathbf{S}_l \mathbf{S}_l^H \mathbf{P}_l^H \Delta$, $\forall i \in \{1, 2, \dots, N_t\}$ and $\forall l \in \mathcal{L}$.

Proof: Please see Appendix VII-B. ■

Using Proposition 3, the constraint (30d) can be written as

$$\left\| \sum_{l \in \mathcal{L}} \sum_{i=1}^{N_t} (\mu_{i,l} \mathbf{F}_{i,l} \mathbf{Y} \mathbf{F}_{i,l}^H + \Sigma \mathbf{E}_i \mathbf{Y} \mathbf{E}_i) - \mathbf{U} \right\|_2 \leq \tau. \quad (46)$$

Finally, we relax the constraint (30c) and write

$$0 \leq \mathbf{Y}_l(i, j) \leq 1, \quad i, j \in \{1, 2, \dots, N_t\}, \quad (47)$$

where $\mathbf{Y}_l(i, j)$ represents the element of the matrix \mathbf{Y} at the i -th column and j -th row.

The resulting problem formulation is written as

$$\begin{aligned} \max_{t, \mathbf{C}', \mathbf{Y}, \alpha, \beta, \gamma, \omega, \nu, \kappa} \quad & t \\ \text{s.t.} \quad & \mathbf{Y} \succeq 0, \end{aligned} \quad (48a)$$

$$(42a), (42b), (42c), (41d), (43),$$

$$(40a), (40b), (37c), (47), (46), (44), \quad (48b)$$

where the vectors α , γ , ω , ν , and κ are composed of the elements α_l , $\gamma_{k,l}$, $\omega_{k,l}$, $\nu_{k,l}$, and $\kappa_{k,l}$, respectively, $\forall k \in \mathcal{K}$ and $\forall l \in \mathcal{L}$. The rank-1 constraint for \mathbf{Y} is removed in accordance with the SDR procedure and the problem is in an iterative fashion by means of interior-point methods. The SCA/SDR-based algorithm to solve the problem (48) is given in Alg. 3.

Proposition 4: Consider the problem (30) with the RF chain selection indicator constraint (30c) relaxed as $0 \leq \lambda_i \leq 1$,

Algorithm 4: AO-Based Algorithm

```

t ← 0, λi0 ← 1, v0, u0, w0, B
while |EEt - EEt-1| > εr do
    ωt ← updateWeights(ut, Λt)
    gt ← updateFilters(ut, Λt)
    Λt+1 ← ALG3(b, ut+1)
    [ut+1, wt+1] ← ALG1(b, Λt, ut, wt, ωt, gt)
    EEt+1 ← updateEE(ut+1, Λt)
    t ← t + 1
end
return ut, Λt.

```

$\forall i \in \{1, 2, \dots, N_t\}$. For the case a rank-1 solution exists for problem (48) and for given \mathbf{P} , the proposed algorithm in Alg. 3 converges to a stationary point of the problem (30) with the relaxed RF chain selection indicator constraint.

Proof: Since the solutions \mathbf{C}' and \mathbf{Y} at iteration $t - 1$ are also feasible solutions for (48) at iteration t , the EE^t is non-decreasing with t and is bounded above due to the per antenna power constraints, per antenna RF chain power consumption and the constant terms P_{BB} and P_{syn} in $\mathcal{E}(\mathbf{P}, \mathbf{A}, \mathbf{B})$ [45], [51], which guarantees the convergence of the algorithm [50, Sec. IV-F].

Assuming a rank-1 solution exists, the optimal solution \mathbf{A} at iteration t obtained by the SDR algorithm is a stationary point of problem (30), since problem (48) is a convex approximation of problem (30) (for which the stationary points can be obtained by SDR [49]) and the KKT conditions of problem (30) are maintained at the point \mathbf{A} . Consequently, we obtain a stationary point of the original problem when the solution point \mathbf{A} at iteration t is the same as the solution point at iteration $t - 1$. ■

D. Proposed AO-Based Algorithm for Optimal Precoder Calculation and RF Chain Selection

We can now move to combine the algorithms Alg. 2 and 3 to solve the problem (16). The proposed algorithm is given in Alg. 4. The algorithm alternates between updating the precoders and RF chain selection indicators until a stopping condition is satisfied.

Proposition 5: Consider the problem (16) with the constraint (16d) relaxed as relaxed as $0 \leq \lambda_i \leq 1$, $\forall i \in \{1, 2, \dots, N_t\}$. For the case a rank-1 solution exists for problem (48), the proposed algorithm in Alg. 4 converges to a stationary point of the problem (16) with the relaxed RF chain selection indicator constraint.

Proof: The convergence of the algorithms given in Alg. 2 and 3 were discussed in the corresponding sections. It follows from the convergence of the employed algorithms that EE^t increases monotonically and is upper bounded due to the per antenna power constraints, per antenna RF chain power consumption and the constant terms P_{BB} and P_{syn} in $\mathcal{E}(\mathbf{P}, \mathbf{A}, \mathbf{B})$ [45], [51]. Assuming a rank-1 solution exists for problem (48), the obtained optimal solutions \mathbf{u}^{t-1} and \mathbf{A}^{t-1} are stationary points of problem (16) with the constraint (16d) relaxed as $0 \leq \lambda_i \leq 1$, $\forall i \in \{1, 2, \dots, N_t\}$, since the AO algorithm is also a special instance of the SCA method [23] and the

KKT conditions of the problem (16) (with the constraint (16d) relaxed) are maintained at the points \mathbf{u}^{t-1} and $\mathbf{\Lambda}^{t-1}$. Consequently, we obtain a stationary point of the original problem (with the constraint (16d) relaxed) when the solution points \mathbf{u}^t and $\mathbf{\Lambda}^t$ are the same as the solution points \mathbf{u}^{t-1} and $\mathbf{\Lambda}^{t-1}$, respectively. ■

We note that the solution $\mathbf{\Lambda}^t$ is a relaxed version of the actual indicator matrices. Obviously, if the indicators $\lambda_i \in \{0, 1\}$, $\forall i \in \{1, 2, \dots, N_t\}$, the obtained solution is also optimal for the non-relaxed problem. Otherwise, we apply a rounding with respect to a threshold to obtain the actual indicators as given below:

$$\lambda'_i = \begin{cases} 0, & \text{if } \lambda_i \leq \tau' \\ 1, & \text{otherwise.} \end{cases} \quad (49)$$

E. Covariance Matrix Design for Enabling Radar Operations

In this section, we investigate specific covariance matrices to enable different radar operation modes, specifically target detection and parameter estimation.

1) Detection Probability

Consider a joint communications and radar signal which consists of L samples in a PRI. The signal, denoted by $\mathbf{x}_l \forall l \in \mathcal{L}$, satisfies $\sum_{l \in \mathcal{L}} \|\mathbf{x}_l\|^2 = N_t$. Note that a such a signal transmitted from a MIMO radar has the property $\mathbf{R}_{\mathbf{x}} = \mathbf{I}_{N_t}$. Let us denote the steering vector at angle θ by $\mathbf{a}(\theta) = [1, e^{j2\pi \sin(\theta)d}, \dots, e^{j2\pi(N_t-1)\sin(\theta)d}]^T$, where d the normalized distance between adjacent array elements with respect to wavelength.

The signal at the radar receiver is written as

$$\mathbf{y}_l^r = \alpha_r \mathbf{a}(\theta) \mathbf{a}(\theta)^T \mathbf{x}_l + \mathbf{n}_l = \alpha_r A(\theta) \mathbf{x}_l + \mathbf{n}_l, \quad (50)$$

where α_r is the complex path loss including the propagation loss and the coefficient of reflection, $A(\theta)$ is the transmit-receive steering matrix and $\mathbf{n}_l \sim \mathcal{CN}(\mathbf{0}, \sigma_n^2 \mathbf{I}_{N_t})$ is the additive Gaussian noise [42]. The detection probability for a target at angle θ is written as

$$P_D = 1 - F_{\chi_2^2(\rho)} \left(F_{\chi_2^2}^{-1}(1 - P_F) \right), \quad (51)$$

where P_F is the false alarm probability, $F_{\chi_2^2}^{-1}$ is the inverse of central chi-squared distribution function with two degrees of freedom, $F_{\chi_2^2(\rho)}$ is the noncentral chi-squared distribution function with two degrees of freedom and noncentrality parameter $\rho \triangleq \frac{|\alpha_r|^2}{\sigma_n^2} |\mathbf{a}^H(\theta) \mathbf{R}_{\mathbf{x}}^T \mathbf{a}(\theta)|^2$ [42].

Next, we move to obtain the detection probability for the quantized RSMA joint communications and radar signal. Proposition 4 gives the detection probability for the considered signal model.

Proposition 4: For large L , the detection probability for the quantized RSMA joint communications and radar signal can be approximately obtained as

$$P_D \approx 1 - F_{\chi_2^2(\rho_{quant})} \left(F_{\chi_2^2}^{-1}(1 - P_F) \right). \quad (52)$$

The non-centrality parameter ρ_{quant} is expressed as

$$\rho_{quant} \triangleq \frac{|\alpha_r|^2 P_{ant} L}{\sigma_n^2} |\mathbf{a}^H(\theta) \mathbf{R}_{\mathbf{x}}^T(\mathbf{P}, \mathbf{\Lambda}, \mathbf{B}) \mathbf{a}(\theta)|^2, \quad (53)$$

where $\check{\mathbf{x}}_l \triangleq \frac{1}{\sqrt{L P_{ant}}} \check{\mathbf{x}}_l$.

Proof: Please see Appendix VII-C. ■

One can immediately observe that $\mathbf{R}_{\check{\mathbf{x}}} = \mathbf{R}_{\check{\mathbf{x}}}/(P_{ant}L)$. The detection probability is maximized when $\mathbf{R}_{\check{\mathbf{x}}}$ converges to the identity matrix. Consequently, the reference matrix to maximize detection probability, \mathbf{U}_{det} , is chosen as

$$\mathbf{U}_{det} = P_{ant} \mathbf{L} \mathbf{I}_{N_t}. \quad (54)$$

2) Parameter Estimation

Consider the scenario in which the radar operates in the tracking mode with N_{tar} targets at angles $\{\theta_1, \theta_2, \dots, \theta_{N_{tar}}\}$. The typical desired beamformer for such a scenario is given as [54]

$$\mathbf{F}_{rad} = \begin{bmatrix} \mathbf{v}_1 & \mathbf{0} & \dots & \mathbf{0} \\ \mathbf{0} & \mathbf{v}_2 & \dots & \mathbf{0} \\ \vdots & \vdots & \ddots & \vdots \\ \mathbf{0} & \mathbf{0} & \dots & \mathbf{v}_{N_{tar}} \end{bmatrix}, \quad (55)$$

where $\mathbf{v}_m \in \mathbb{C}^{N_{tar} \times 1}$ is composed of the entries of $\mathbf{a}(\theta_m)$, $\forall m \in \{1, 2, \dots, N_{tar}\}$, at the corresponding antennas. Then, the corresponding reference covariance matrix is written as

$$\mathbf{U}_{est} = P_{ant} L \mathbf{F}_{rad} \mathbf{F}_{rad}^H. \quad (56)$$

A performance metric for the target parameter estimation is the Cramer-Rao Bound (CRB) for the parameter in consideration. An example is the estimation of Direction of Arrival (DOA), which is given for a single target as in (57) [55]. The matrix $\dot{\mathbf{A}}(\theta)$ in (57) is the derivation of $\mathbf{A}(\theta)$ with respect to θ and $\text{SNR} = \frac{|\alpha_r|^2 P_{ant} L}{\sigma_n^2}$ from (74).

F. Complexity Analysis

We calculate the complexity of the proposed algorithm at each iteration by calculating the complexities of the algorithms **ALG1** and **ALG3** at iteration- t .

1) Complexity of ALG1

The complexity of **ALG1** at each iteration is analyzed in terms of the complexities of the update steps for \mathbf{v}_r and \mathbf{u}_r .

- Update step for \mathbf{v}_r : The complexity of this step is equal to the complexity of interior-point methods for solving (19), which can be written in the equivalent Quadratically Constrained Quadratic Program (QCQP) form

$$\begin{aligned} \min_{\mathbf{v}_r, t} \quad & f(\mathbf{v}_r) + s \\ \text{s.t.} \quad & \sum_{n \in \mathcal{S}} \|\mathbf{v}_{r,n} - \mathbf{u}_{r,n}^t + \mathbf{w}_{r,n}^t\|^2 \leq s, \end{aligned}$$

where s is a slack variable. The complexity of solving such a problem by interior point methods is $\mathcal{O}((L(K+2)N_t+1)^3) = \mathcal{O}((L(K+2)N_t)^3)$, with $\mathcal{O}(\cdot)$ denoting the big O function.

- Update step for \mathbf{u}_r : The complexity of this step is equal to the complexity of SDR method, which is given by $\mathcal{O}((L(K+2)N_t)^{4.5} \log(1/\epsilon))$ for given solution accuracy given a solution accuracy $\epsilon > 0$ [47].

$$\text{CRB}(\theta) = \frac{\text{tr}(\mathbf{A}(\theta)\mathbf{R}_{\mathbf{x}}\mathbf{A}^H(\theta))}{2\text{SNR} \left(\text{tr}(\hat{\mathbf{A}}(\theta)\mathbf{R}_{\mathbf{x}}\hat{\mathbf{A}}^H(\theta))\text{tr}(\mathbf{A}(\theta)\mathbf{R}_{\mathbf{x}}\mathbf{A}^H(\theta)) - |\text{tr}(\mathbf{A}(\theta)\mathbf{R}_{\mathbf{x}}\hat{\mathbf{A}}^H(\theta))|^2 \right)}. \quad (57)$$

Algorithm 5: AO-Based Algorithm (Imperfect CSIT)

```

 $t \leftarrow 0, \lambda_i^0 \leftarrow 1, \mathbf{v}^0, \mathbf{u}^0, \mathbf{w}^0, \mathbf{B}$ 
while  $|\text{EE}^t - \text{EE}^{t-1}| > \epsilon_r$  do
   $(\boldsymbol{\omega}^{(M)})^t \leftarrow \text{updateWeights}(\mathbf{u}^t, \boldsymbol{\Lambda}^t, \mathbb{H}_k^{(M)})$ 
   $(\mathbf{g}^{(M)})^t \leftarrow \text{updateFilters}(\mathbf{u}^t, \boldsymbol{\Lambda}^t, \mathbb{H}_k^{(M)})$ 
   $\boldsymbol{\Lambda}^{t+1} \leftarrow \text{ALG3}(b, \mathbf{u}^{t+1}, \mathbb{H}_k^{(M)})$ 
   $[\mathbf{u}^{t+1}, \mathbf{w}^{t+1}] \leftarrow \text{ALG1}(\mathbf{B}, \boldsymbol{\Lambda}^t, \mathbf{u}^t, \mathbf{w}^t,$ 
     $(\boldsymbol{\omega}^{(M)})^t, (\mathbf{g}^{(M)})^t, \mathbb{H}_k^{(M)})$ 
   $\text{EE}^{t+1} \leftarrow \text{updateEE}(\mathbf{u}^{t+1}, \boldsymbol{\Lambda}^t, \mathbb{H}_k^{(M)})$ 
   $t \leftarrow t + 1$ 
end
return  $\mathbf{u}^t, \boldsymbol{\Lambda}^t$ 

```

Therefore, the complexity of a single iteration of **ALG1** is dominated by that of SDR method, and the overall complexity is written as

$$\mathcal{C}_{\text{ALG1}} = \mathcal{O}(T_{1,t}(L(K+2)N_t)^{4.5} \log(1/\epsilon)), \quad (59)$$

where $T_{1,t}$ denotes the number of iterations of **ALG1** at iteration- t .

2) Complexity of **ALG3**

Omitting the constraint (16e), it is easy to see that the complexity of **ALG3** is equal to the complexity of applying SDR method to solve an optimization problem, with an optimization vector of length- N_t and $(3+5KL+2N_t)$ constraints. Therefore, we approximate the complexity of **ALG3** as

$$\mathcal{C}_{\text{ALG3}} \approx \mathcal{O}(T_{3,t}(3+5KL+2N_t)^4 \sqrt{N_t} \log(1/\epsilon)), \quad (60)$$

where $T_{3,t}$ denotes the number of iterations of **ALG3** at iteration- t [47].

3) Complexity of Proposed Algorithm

Assuming the same solution accuracy for **ALG1** and **ALG3**, the overall complexity of the proposed algorithm at iteration- t can be approximately written as

$$\mathcal{C}_{\text{prop},t} \approx \mathcal{O}([T_{1,t}(L(K+2)N_t)^{4.5} + T_{3,t}(3+5KL+2N_t)^4 \sqrt{N_t}] \log(1/\epsilon)). \quad (61)$$

IV. FORMULATION UNDER IMPERFECT CSIT

In this section, we consider the case when the transmitter has imperfect CSIT. In the case of imperfect CSIT, the transmitter uses the imperfect channel estimates for precoder calculation instead of the perfect CSI. Let $\hat{\mathbf{h}}_k$ denote the CSIT for user- k . The instantaneous channel is written in terms of CSIT as

$$\mathbf{h}_k = \sqrt{1-\sigma_{ce}^2} \hat{\mathbf{h}}_k + \sigma_{ce} \tilde{\mathbf{h}}_k, \quad (62)$$

where $\tilde{\mathbf{h}}_{k,n}$ is the channel estimation error. The entries of $\hat{\mathbf{h}}_{k,n}$ and $\tilde{\mathbf{h}}_{k,n}$ are independent.

Ergodic rates $\mathbb{E}_{\mathbf{h}_k} \{R_k\}$ and $\mathbb{E}_{\mathbf{h}_k} \{R_{c,k}\}$ are considered for precoder design instead of the instantaneous rates in order to achieve robust communications under imperfect CSIT [23]. Therefore, it is of interest to investigate the EE behaviour and optimal number of quantization bits and active RF chains for the practical case of imperfect CSIT. Let us define the average rates $\bar{R}_k = \mathbb{E}_{\mathbf{h}_k | \hat{\mathbf{h}}_k} \{R_k\}$ and $\bar{R}_{c,k} = \mathbb{E}_{\mathbf{h}_k | \hat{\mathbf{h}}_k} \{R_{c,k}\}$. It has been shown in [23] that the ergodic rates can be expressed in terms of the average rates as $\mathbb{E}_{\mathbf{h}_k} \{R_k\} = \mathbb{E}_{\hat{\mathbf{h}}_k} \{\bar{R}_k\}$ and $\mathbb{E}_{\mathbf{h}_k} \{R_{c,k}\} = \mathbb{E}_{\hat{\mathbf{h}}_k} \{\bar{R}_{c,k}\}$. We define $\bar{\mathcal{E}}(\mathbf{P}, \boldsymbol{\Lambda}, \mathbf{B}) = \frac{\frac{1}{L} \sum_{l \in \mathcal{L}} (\bar{C}_l(\mathbf{P}_l, \boldsymbol{\Lambda}, \mathbf{B}) + \sum_{k \in \mathcal{K}} \bar{R}_{k,l}(\mathbf{P}_l, \boldsymbol{\Lambda}, \mathbf{B}))}{P_{\text{tot}}(\boldsymbol{\Lambda}, \mathbf{B})}$ and write the problem (16) in terms of the average rates as

$$\max_{\mathbf{C}, \mathbf{P}, \boldsymbol{\Lambda}} \bar{\mathcal{E}}(\mathbf{P}, \boldsymbol{\Lambda}, \mathbf{B}) \quad (63a)$$

$$\text{s.t. } \bar{C}_l(\mathbf{P}_l, \boldsymbol{\Lambda}, \mathbf{B}) \leq \bar{R}_{c,k,l}(\mathbf{P}_l, \boldsymbol{\Lambda}, \mathbf{B}), \quad k \in \mathcal{K}, \forall l \in \mathcal{L} \quad (63b)$$

$$\bar{R}_{\text{sum}}(\mathbf{P}, \boldsymbol{\Lambda}, \mathbf{B}) \geq R_{\text{th}} \quad (63c)$$

$$(16d), (16e), (16g). \quad (63d)$$

Solving (63) for each given $\hat{\mathbf{h}}_k, \forall k \in \mathcal{K}$, and averaging the solutions over $\hat{\mathbf{h}}_k$, we obtain $\mathbb{E}_{\hat{\mathbf{h}}_k} \{\bar{\mathcal{E}}\} = \frac{\frac{1}{L} \sum_{l \in \mathcal{L}} (\mathbb{E}_{\hat{\mathbf{h}}_k} \{\bar{C}_l\} + \sum_{k \in \mathcal{K}} \mathbb{E}_{\hat{\mathbf{h}}_k} \{\bar{R}_{k,l}\})}{P_{\text{tot}}(\boldsymbol{\Lambda}, \mathbf{B})}$, i.e., EE in terms of the ergodic sum rate. The stochastic problem (63) can be solved by writing its deterministic equivalent using the Sample Average Approximation (SAA) method [56]. We define the sample set for given $\hat{\mathbf{h}}_k$ and $\mathcal{M} = \{1, 2, \dots, M\}$ as

$$\mathbb{H}_k^{(M)} \triangleq \left\{ \mathbf{h}_k^{(m)} = \hat{\mathbf{h}}_k + \tilde{\mathbf{h}}_k^{(m)} \mid \hat{\mathbf{h}}_k, m \in \mathcal{M} \right\}, \quad (64)$$

where the elements are independent and identically distributed with $f_{\mathbf{h} | \hat{\mathbf{h}}}(\mathbf{h} | \hat{\mathbf{h}})$. This set is used to approximate the average rates by their Sample Average Functions (SAFs) as

$$\begin{aligned} \bar{R}_{c,k,l}^{(M)}(\mathbf{P}_l, \boldsymbol{\Lambda}, \mathbf{B}) &= \frac{1}{M} \sum_{m=1}^M R_{c,k,l}^{(m)}(\mathbf{P}_l, \boldsymbol{\Lambda}, \mathbf{B}, \mathbf{h}_k^{(m)}), \\ \bar{R}_{k,l}^{(M)}(\mathbf{P}_l, \boldsymbol{\Lambda}, \mathbf{B}) &= \frac{1}{M} \sum_{m=1}^M R_{k,l}^{(m)}(\mathbf{P}_l, \boldsymbol{\Lambda}, \mathbf{B}, \mathbf{h}_k^{(m)}), \end{aligned} \quad (65)$$

where $R_{c,k,l}^{(m)}(\mathbf{P}_l, \boldsymbol{\Lambda}, \mathbf{B}, \mathbf{h}_k^{(m)})$ and $R_{k,l}^{(m)}(\mathbf{P}_l, \boldsymbol{\Lambda}, \mathbf{B}, \mathbf{h}_k^{(m)})$ are the rates obtained by the m th channel realization $\mathbf{h}_k^{(m)}$.

The updated algorithm to solve the problem for imperfect CSIT is given in Alg. 5. Comparing the updated algorithm with Alg. 4, the difference is the use of channel samples in the set $\mathbb{H}_k^{(M)}$ for each calculation. First, we take a look at the changes in the precoder update step. The samples are used in **ALG1** (Alg. 1) at the update step for \mathbf{v}_r^{t+1} . The solution of the MSE minimization problem in the considered step can be obtained in a similar way that is described in [37], [38].

Next, we describe the modifications for the RF chain selection procedure. The use of $\bar{R}_{c,k,l}^{(M)}(\mathbf{P}_l, \boldsymbol{\Lambda}, \mathbf{B})$ and $\bar{R}_{k,l}^{(M)}(\mathbf{P}_l, \boldsymbol{\Lambda}, \mathbf{B})$ in the formulation (30) results in taking the

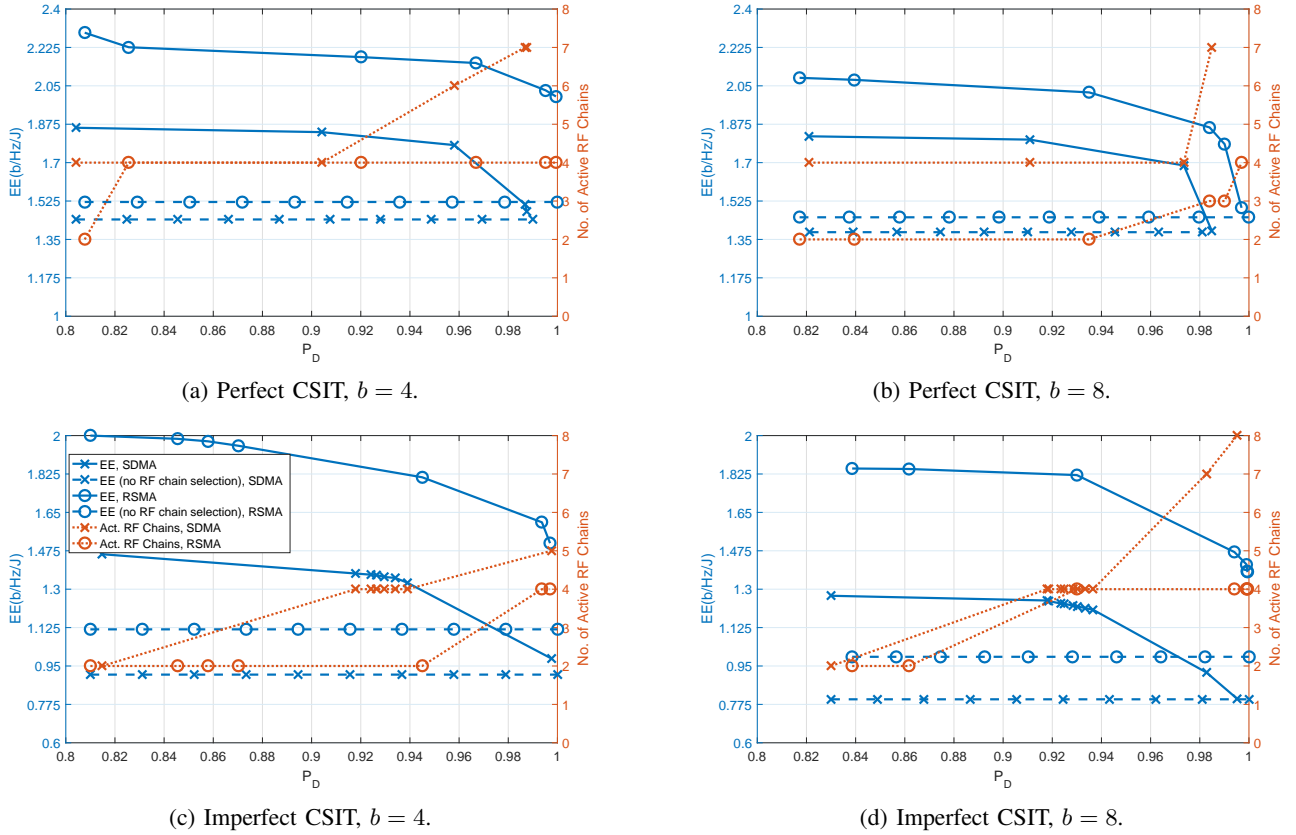


Fig. 2: Average detection probability P_D vs. EE performance of SDMA and RSMA, $SR > 10$ b/s/Hz (perfect CSIT), $SR > 5$ b/s/Hz (imperfect CSIT), $P_F = 10^{-7}$, single target, $N_t = 8$, $K = 2$, $L = 10$, $\alpha_r = 0.1$.

averages of the logarithmic terms in the formulation (36), which respectively translate the constraints (42b), (42c), (41d), (40a), (40b), (37c), (44) in (48) to the ones given below:

$$\text{tr}(\mathbf{\Upsilon}\mathbf{\Psi}_k^{(m)}) \leq e^{(\gamma_{k,l}^{(m)})^{t-1}} (\gamma_{k,l}^{(m)} - (\gamma_{k,l}^{(m)})^{t-1} + 1), \quad (66a)$$

$$\text{tr}(\mathbf{\Upsilon}\mathbf{\Omega}_k^{(m)}) \geq e^{\kappa_{k,l}^{(m)}}, \quad (66b)$$

$$\alpha_l^2 - \bar{C}'_l - \frac{1}{M} \sum_{k \in \mathcal{K}} \sum_{m \in \mathcal{M}} \kappa_{k,l}^{(m)} + \frac{1}{M} \sum_{k \in \mathcal{K}} \sum_{m \in \mathcal{M}} \gamma_{k,l}^{(m)} \leq 0, \quad (66c)$$

$$\text{tr}(\mathbf{\Upsilon}\mathbf{\Gamma}_k^{(m)}) \leq e^{(\omega_{k,l}^{(m)})^{t-1}} (\omega_{k,l}^{(m)} - (\omega_{k,l}^{(m)})^{t-1} + 1), \quad (66d)$$

$$\text{tr}(\mathbf{\Upsilon}\mathbf{\Xi}_k^{(m)}) \geq e^{\nu_{k,l}^{(m)}}, \quad (66e)$$

$$\bar{C}'_l - \frac{1}{M} \sum_{m \in \mathcal{M}} \nu_{k,l}^{(m)} + \frac{1}{M} \sum_{m \in \mathcal{M}} \omega_{k,l}^{(m)} \leq 0, \quad (66f)$$

$$\frac{1}{L} \sum_{l \in \mathcal{L}} \bar{C}'_l + \frac{1}{L} \sum_{l \in \mathcal{L}} \frac{1}{M} \sum_{k \in \mathcal{K}} \sum_{m \in \mathcal{M}} \kappa_{k,l}^{(m)} - \frac{1}{L} \sum_{l \in \mathcal{L}} \frac{1}{M} \sum_{k \in \mathcal{K}} \sum_{m \in \mathcal{M}} \gamma_{k,l}^{(m)} \geq \ln 2R_{th}, \quad (66g)$$

where the matrices with upper-script (m) are calculated using the corresponding channel ensemble $\mathbf{h}_k^{(m)}$.

TABLE I: Simulation parameters

Parameter	Value	Parameter	Value
N_t	8	$P_{BB}[W]$	1
K	2	$P_{circ}[W]$	1
L	10	$P_{syn}[W]$	2
d	0.5	$P_{DAC}[mW]$	1
$P_{ant}[mW]$	125	$p_{int}[mW]$	25
$N_0[mW]$	1	$S_{DAC}[Mbps]$	125
σ_{ce}	0.2	η_{PA}	0.39

The updated problem formulation is written as

$$\begin{aligned} & \max_{t, \mathbf{C}', \mathbf{\Upsilon}, \alpha, \beta, \gamma, \omega, \nu, \kappa} t \\ & \text{s.t. } \mathbf{\Upsilon} \succeq 0, \end{aligned} \quad (67a)$$

$$\begin{aligned} & (42a), (66a), (66b), (66c), (43), \\ & (66d), (66e), (66f), (66g), (47), (46). \end{aligned} \quad (67b)$$

Similar to the problem (48), the problem (67b) can be solved by Alg. 3.

Finally, we analyze the complexity of the proposed algorithm for imperfect CSIT. Following the analysis for the perfect CSIT case, the complexity of the proposed algorithm for imperfect CSIT can be calculated in a straightforward

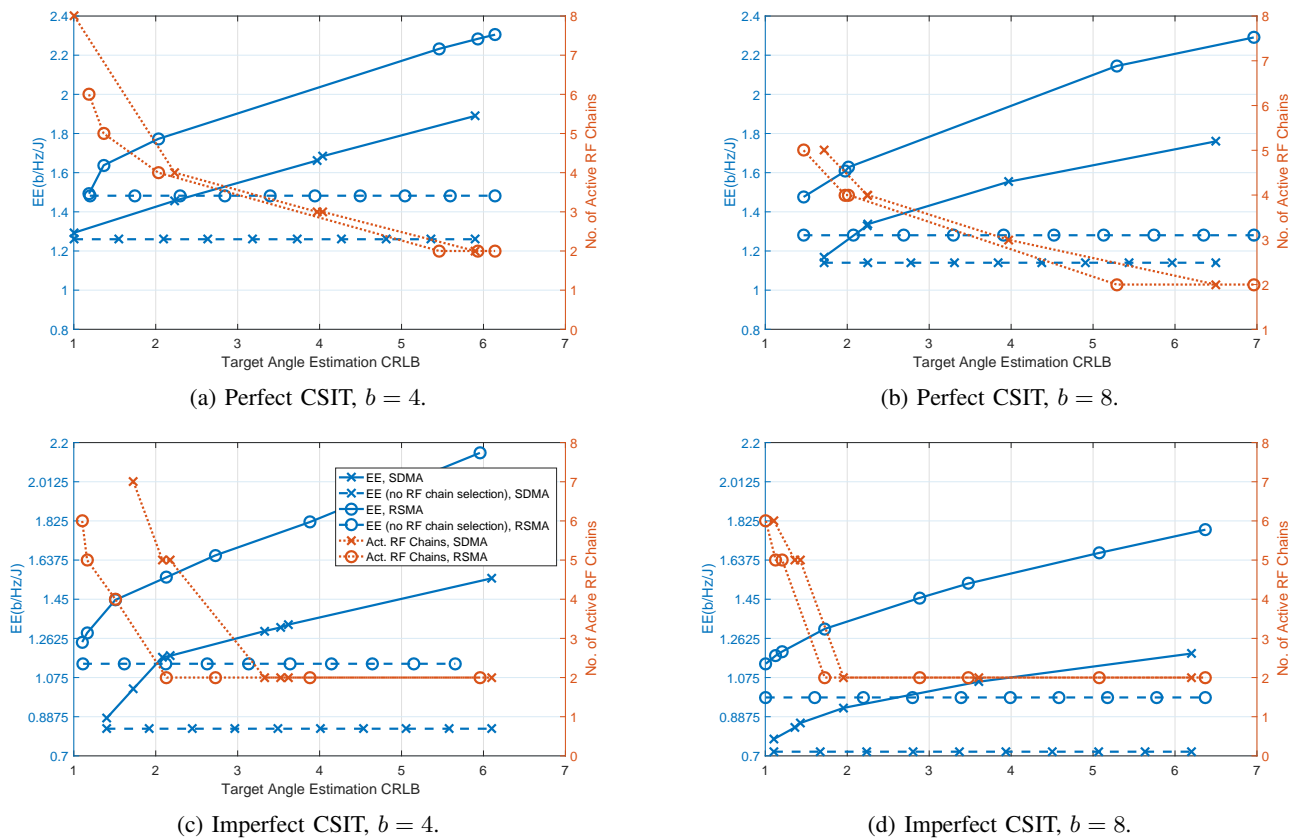


Fig. 3: Target angle estimation CRLB vs. EE performance of SDMA and RSMA, $SR > 5$ b/s/Hz, $P_F = 10^{-7}$, single target, $N_t = 8$, $K = 2$, $L = 10$, $\alpha_r = 0.1$, $\theta = \pi/4$.

manner as

$$C'_{prop,t} \approx \mathcal{O}([T_{1,t}(L(K+2)N_t)^{4.5} + T_{3,t}(3 + 5KL + 2N_t)^4 M^4 \sqrt{N_t}] \log(1/\epsilon)). \quad (68)$$

V. SIMULATION RESULTS

In this section, we present simulation results to investigate the performance of RSMA using the proposed algorithm and perform comparisons with the performance of SDMA. The optimal precoders for SDMA can be obtained by turning off the common stream in the optimization problem formulation and solving by the proposed algorithm. We analyze the EE performance of the system with the optimized precoders with respect to the communications and radar performance metrics. The parameters used in the simulations are given in Table I.

We start by investigating the EE performance of the system with respect to radar metrics in detection and tracking modes. Fig. 2 shows the EE performance with respect to average detection probability for $b = \{4, 8\}$, $P_F = 10^{-7}$, and $SR > 10$ b/s/Hz under perfect and imperfect CSIT. We study the detection performance for a single target and the reference covariance matrix is set as \mathbf{I}_{N_t} . The curves shown in Fig. 2 are obtained by running simulations for $\tau = \{1, 1.5, \dots, 8\}$ and $R_{th} = 1$ b/s/Hz, and picking the best performance points that satisfy $SR > 10$ b/s/Hz.

For a better convergence performance, the covariance matrix distance constraint (16e) is modified to consider the distance only between the diagonal elements of the designed and reference covariance matrices due to the sparse nature of the reference matrix. The CSIT error vector in (62) is assumed to have i.i.d. complex Gaussian elements of unit variance. The figures also show the number of active transmit antennas to achieve the demonstrated performance for each scheme. One can immediately observe that RSMA achieves a higher EE than SDMA for all considered scenarios. RSMA satisfies the communications and radar performance metric constraints with fewer number of active antennas, resulting in a higher EE with both perfect and imperfect CSIT. The capability of RSMA to activate fewer antennas than SDMA stems from its higher degrees of freedom in design space due to the additional common stream and its improved sum-rate performance under interference.

Comparing the performance with different numbers of quantization bits, one can notice that EE decreases when the b is increased from 4 to 8. Although the sum-rate achieved with $b = 8$ is higher due to lower quantization noise and higher multiplicative quantization gain δ , the power consumption is also higher, resulting in a lower EE than that of $b = 4$.

Next, we investigate the performance in the tracking mode of the radar system. Fig. 3 shows the EE performance with respect to CRLB for $b = \{4, 8\}$, $P_F = 10^{-7}$, and $SR > 5$

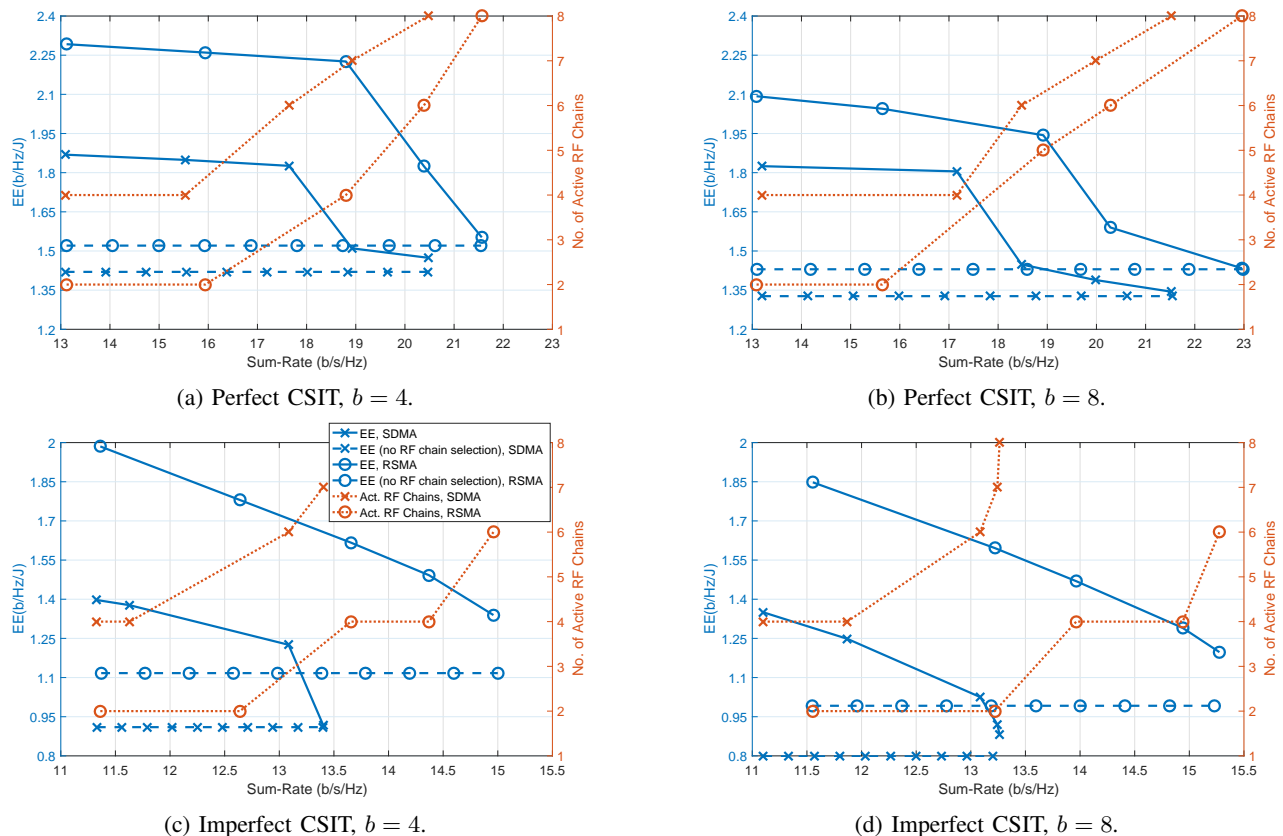


Fig. 4: SR vs. EE performance of SDMA and RSMA, $\bar{P}_D > 0.8$, $P_F = 10^{-7}$, $N_t = 8$, $K = 2$, single target, $L = 10$, $\alpha_r = 0.1$.

b/s/Hz under perfect and imperfect CSIT. We consider the angle estimation performance for a single target at angle $\pi/4$ and the reference covariance matrix is set as $\mathbf{a}(\pi/4)\mathbf{a}(\pi/4)^H$. The curves shown in Fig. 2 are obtained by running simulations for $\tau = \{45, 46, \dots, 70\}$ and $R_{th} = 0.5$ b/s/Hz, and picking the best performance points that satisfy $SR > 5$ b/s/Hz. Similar to the case in detection performance, RSMA achieves higher EE than SDMA under both perfect and imperfect CSIT. The number of active antennas used to achieve a given CRLB performance are similar with RSMA and SDMA, as opposed to the case with average detection probability. This is due to the reference covariance matrix for minimizing CRLB being a non-sparse matrix. This, in turn, requires higher number of active antennas to decrease the distance between the designed and reference covariance matrix and reduce CRLB for both RSMA and SDMA.

Next, we analyze the communications system performance. Fig. 4 shows the EE performance with respect to sum-rate for $b = \{4, 8\}$, $P_F = 10^{-7}$, and $\bar{P}_D > 0.8$ under perfect and imperfect CSIT. As in the simulations for Fig. 2, the curves shown in Fig. 2 are obtained by running simulations for $\tau = \{1, 1.5, \dots, 8\}$ and $R_{th} = 1$ b/s/Hz, and picking the best performance points that satisfy $\bar{P}_D > 0.8$ b/s/Hz. For a better convergence performance, the covariance matrix distance constraint (16e) is modified to consider the distance only between the diagonal elements of the designed and reference covariance matrices due to the sparse nature of the reference matrix.

Similar to the case in radar metrics, RSMA achieves a higher EE while achieving similar sum-rate performance compared to SDMA. Consequently, we can conclude that RSMA can achieve a higher EE while guaranteeing a given radar and communications performance, owing to its larger design space and improved interference management capabilities.

Finally, we investigate the change in performance metrics with varying similarity threshold values. As an example, Fig. 5a shows the change in target angle estimation CRLB achieved by RSMA with respect to τ for $b = 8$ under imperfect CSIT. As expected, the CRLB increases with increasing τ . The EE also increases with τ , as increasing τ relaxes the similarity constraint and allows the system to deactivate several antennas to improve EE. Fig. 5b shows the beam pattern for communicating with 2 users and tracking a target at $\theta = \pi/4$ for various τ values. One can see that the main lobe of the signal shifts from $\theta = \pi/4$ and the sidelobe power increases as τ increases. This enables the system to operate with higher EE with a penalty in estimation performance.

VI. CONCLUSION

In this work, we consider RSMA for multi-antenna DFRC systems with low-resolution DACs. We investigate the EE performance of the proposed system with optimal RF chain selection under communications and radar performance constraints and under imperfect CSIT. We formulate a non-convex EE maximization problem and propose an iterative algorithm

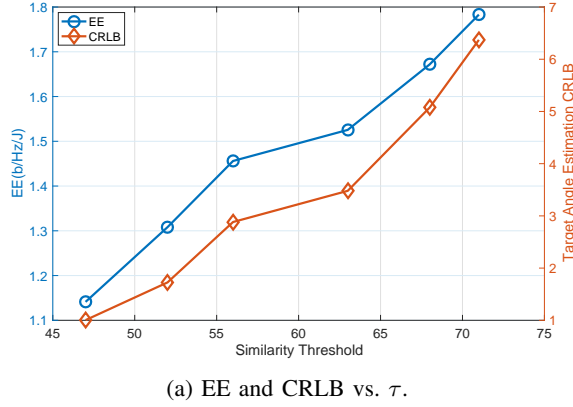
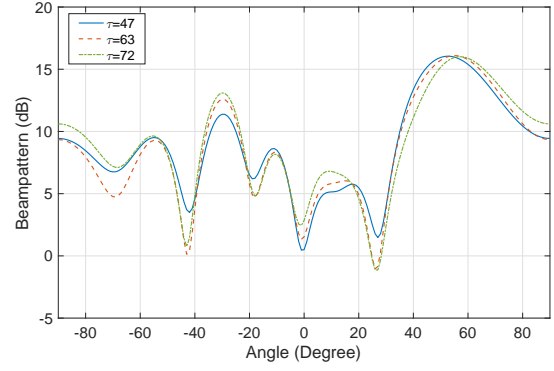
(a) EE and CRLB vs. τ .(b) Beampattern with varying τ .

Fig. 5: Performance metrics vs. τ , RSMA, imperfect CSIT, $SR > 5$ b/s/Hz, $P_F = 10^{-7}$, single target, $N_t = 8$, $K = 2$, $L = 10$, $\alpha_r = 0.1$, $\theta = \pi/4$.

to solve it. We prove the convergence of the proposed algorithm by analytical means. We perform simulations to compare the performance of RSMA and SDMA in terms of EE, communications, and radar metrics. The results show RSMA can achieve a higher EE both under perfect and imperfect CSIT by means of activating less number of antennas than SDMA, which is enabled by the larger design space and improved interference management capabilities of RSMA.

VII. APPENDIX

A. Proof of Proposition 1

In the following derivations, we consider the following assumption.

Assumption: The quantization noise is a Wide-Sense Stationary (WSS) stochastic process and ergodic in the wide sense, i.e., $\mathbb{E}\{\epsilon_l\} = \mathbf{0}_{N_t}$, $\mathbb{E}\{\epsilon_l \epsilon_l^H\} = \Sigma$, and

$$\lim_{L \rightarrow \infty} \frac{1}{L} \sum_{l \in \mathcal{L}} \epsilon_l \rightarrow \mathbf{0}_{N_t}, \quad \lim_{L \rightarrow \infty} \frac{1}{L} \sum_{l \in \mathcal{L}} \epsilon_l \epsilon_l^H \rightarrow \Sigma, \quad (69)$$

where the convergence is in squared mean [57].

With the assumption above, we write

$$\begin{aligned} & \sum_{l \in \mathcal{L}} \tilde{\mathbf{x}}_l \tilde{\mathbf{x}}_l^H \\ &= \sum_{l \in \mathcal{L}} \Delta \Lambda \mathbf{P}_l \mathbf{s}_l \mathbf{s}_l^H \mathbf{P}_l^H \Lambda \Delta + \sum_{l \in \mathcal{L}} \Delta \Lambda \mathbf{P}_l \mathbf{s}_l \epsilon_l^H \Lambda \quad (70a) \\ &+ \sum_{l \in \mathcal{L}} \Lambda \epsilon_l \mathbf{s}_l^H \mathbf{P}_l^H \Lambda \Delta + \sum_{l \in \mathcal{L}} \Lambda \epsilon_l \epsilon_l^H \Lambda \quad (70b) \\ &\approx \sum_{l \in \mathcal{L}} \Delta \Lambda \mathbf{P}_l \mathbf{s}_l \mathbf{s}_l^H \mathbf{P}_l^H \Lambda \Delta + L \Lambda \mathbb{E}\{\epsilon_l \epsilon_l^H\} \Lambda \quad (70c) \\ &= \sum_{l \in \mathcal{L}} \Delta \Lambda \mathbf{P}_l \mathbf{s}_l \mathbf{s}_l^H \mathbf{P}_l^H \Lambda \Delta + L \Lambda \Sigma \Lambda \quad (70d) \\ &\triangleq \bar{\mathbf{R}}_{\tilde{\mathbf{x}}}(\mathbf{P}, \Lambda, \mathbf{B}). \quad (70e) \end{aligned}$$

where the approximation in (70c) uses the ergodicity of the stochastic process.

B. Proof of Proposition 3

It is easy to see that the matrix $\mathbf{A}_l = \Delta \mathbf{P}_l \mathbf{s}_l \mathbf{s}_l^H \mathbf{P}_l^H \Lambda$ is a positive semi-definite matrix, as $\mathbf{b}^H \mathbf{A}_l \mathbf{b} \geq 0$ for any $\mathbf{b} \in \mathbb{C}^{N_t \times 1}$. Consequently, we can express \mathbf{A}_l in terms of its eigenvalue decomposition, such that

$$\mathbf{A}_l = \sum_{i=1}^{N_t} \mu_{i,l} \mathbf{f}_{i,l} \mathbf{f}_{i,l}^H, \quad (71)$$

where $\mu_{i,l}$ is the i -th eigenvalue and $\mathbf{f}_{i,l}$ is the i -th eigenvector of \mathbf{A}_l , $\forall i \in \{1, 2, \dots, N_t\}$ and $\forall l \in \mathcal{L}$. Then, we write

$$\begin{aligned} & \bar{\mathbf{R}}_{\tilde{\mathbf{x}}}(\mathbf{P}, \Lambda, \mathbf{B}) \\ &= \sum_{l \in \mathcal{L}} \Delta \Lambda \mathbf{P}_l \mathbf{s}_l \mathbf{s}_l^H \mathbf{P}_l^H \Lambda \Delta + L \Lambda \Sigma \Lambda \quad (72a) \end{aligned}$$

$$= \sum_{l \in \mathcal{L}} \Lambda \Delta \mathbf{P}_l \mathbf{s}_l \mathbf{s}_l^H \mathbf{P}_l^H \Lambda \Delta + L \Lambda \Sigma \Lambda \quad (72b)$$

$$= \sum_{l \in \mathcal{L}} \Lambda \mathbf{A}_l \Lambda + L \Lambda \Sigma \Lambda \quad (72c)$$

$$= \sum_{l \in \mathcal{L}} \Lambda \left(\sum_{i=1}^{N_t} \mu_{i,l} \mathbf{f}_{i,l} \mathbf{f}_{i,l}^H \right) \Lambda + L \Lambda \Sigma \Lambda \quad (72d)$$

$$= \sum_{l \in \mathcal{L}} \sum_{i=1}^{N_t} \mu_{i,l} \mathbf{F}_{i,l} \boldsymbol{\lambda} \boldsymbol{\lambda}^T \mathbf{F}_{i,l}^H + L \sum_{i=1}^{N_t} \Sigma \mathbf{E}_i \boldsymbol{\lambda} \boldsymbol{\lambda}^T \mathbf{E}_i \quad (72e)$$

$$= \sum_{l \in \mathcal{L}} \sum_{i=1}^{N_t} (\mu_{i,l} \mathbf{F}_{i,l} \boldsymbol{\Upsilon} \mathbf{F}_{i,l}^H + \Sigma \mathbf{E}_i \boldsymbol{\Upsilon} \mathbf{E}_i), \quad (72f)$$

where $\mathbf{F}_{i,l} = \text{Diag}(\mathbf{f}_{i,l})$. The expression (72b) follows from $\Lambda \Delta = \Delta \Lambda$ due to both Δ and Λ being diagonal matrices and (72d) follows from the fact that $\mathbf{D}_a \mathbf{b} = \mathbf{D}_b \mathbf{a}$.

C. Proof of Proposition 4

We assume that the random quantization noise is a WSS stochastic process, as in the proof of Proposition 1. Then, we

can write

$$\begin{aligned} & \sum_{l \in \mathcal{L}} \|\check{\mathbf{x}}_l\|^2 \\ &= \sum_{l \in \mathcal{L}} \mathbf{s}_l^H \mathbf{P}_l^H \Lambda \Delta \Delta \Delta \Lambda \mathbf{P}_l \mathbf{s}_l + \sum_{l \in \mathcal{L}} \Delta \Lambda \mathbf{P}_l \mathbf{s}_l \epsilon_l^H \Lambda \\ &+ \sum_{l \in \mathcal{L}} \Lambda \epsilon_l \mathbf{s}_l^H \mathbf{P}_l^H \Lambda \Delta + \sum_{l \in \mathcal{L}} \epsilon_l^H \Lambda \Lambda \epsilon_l \end{aligned} \quad (73a)$$

$$= \sum_{l \in \mathcal{L}} \mathbf{s}_l^H \mathbf{P}_l^H \Lambda \Delta \Delta \Delta \Lambda \mathbf{P}_l \mathbf{s}_l + \sum_{l \in \mathcal{L}} \Lambda \text{tr}(\epsilon_l \epsilon_l^H) \Lambda \quad (73b)$$

$$\approx \sum_{l \in \mathcal{L}} \text{tr}(\Delta \Lambda \mathbf{P}_l \mathbf{s}_l \mathbf{s}_l^H \mathbf{P}_l^H \Lambda \Delta) + L \Lambda \text{tr}(\mathbb{E}\{\epsilon \epsilon^H\}) \Lambda \quad (73c)$$

$$= L \sum_{i=1}^{N_t} \lambda_i P_{ant} + L \sum_{i=1}^{N_t} \lambda_i \sigma_{e,i}^2 \quad (73d)$$

$$\triangleq \bar{P}_{\mathbf{x}}(\mathbf{P}, \Lambda, \mathbf{B}). \quad (73e)$$

Note that for a system model without DAC quantization or RF chain selection, $\lim_{b \rightarrow \infty} \bar{P}_{\mathbf{x}}(\mathbf{P}, \mathbf{I}_{N_t}, b \mathbf{I}_{N_t}) = N_t L P_{ant}$. In order to write the detection probability for the considered quantized transmit signal with RF chain selection, we introduce the signal $\check{\mathbf{x}}_l \triangleq \sqrt{\frac{N_t}{N_t L P_{ant}}} \tilde{\mathbf{x}}_l$. One can observe that $\lim_{b \rightarrow \infty} \bar{P}_{\mathbf{x}}(\mathbf{P}, \mathbf{I}_{N_t}, b \mathbf{I}_{N_t}) = N_t$ and $\lim_{b \rightarrow \infty} \mathbf{R}_{\check{\mathbf{x}}}(\mathbf{P}, \mathbf{I}_{N_t}, b \mathbf{I}_{N_t}) = \mathbf{I}_{N_t}$ if $\check{\mathbf{x}}_l$ is an orthogonal waveform.

We write the l -th received quantized symbol at the radar receiver using (7), (50) and $\check{\mathbf{x}}_l$ as,

$$\begin{aligned} \tilde{\mathbf{y}}_l^T &= \alpha_r A(\theta) \check{\mathbf{x}}_l + \mathbf{n}_l \\ &= \alpha_r A(\theta) \Delta \Lambda \mathbf{P}_l \mathbf{s}_l + \alpha_r A(\theta) \Lambda \epsilon_l + \mathbf{n}_l \\ &= \alpha_r \sqrt{P_{ant}} L A(\theta) \check{\mathbf{x}}_l + \mathbf{n}_l. \end{aligned} \quad (74)$$

Then, the detection probability for the quantized radar signal can be approximately written as in (51) with the non-centrality parameter expressed as

$$\rho_{quant} \triangleq \frac{|\alpha_r|^2 P_{ant} L}{\sigma_n^2} |\mathbf{a}^H(\theta) \mathbf{R}_{\check{\mathbf{x}}}^T(\mathbf{P}, \Lambda, \mathbf{B}) \mathbf{a}(\theta)|^2. \quad (75)$$

REFERENCES

- [1] Cisco Annual Internet Report 2018-23 White Paper [Online].
- [2] Ericsson Mobility Report, pp. 1-36, June 2021.
- [3] J. G. Andrews et al., "What will 5G be?," *IEEE Journ. Sel. Areas Commun.*, vol. 32, no. 6, pp. 1065-1082, June 2014.
- [4] DARPA. (2016). Shared Spectrum Access for Radar and Communications (SSPARC) [Online]. Available: <https://www.darpa.mil/program/shared-spectrum-access-for-radar-and-communications>
- [5] H. Griffiths et al., "Radar spectrum engineering and management: Technical and regulatory issues," *Proc. IEEE*, vol. 103, no. 1, pp. 85-102, Jan. 2015.
- [6] A. Zappone, et al., "Globally optimal energy-efficient power control and receiver design in wireless networks," *IEEE Trans. Signal Proc.*, vol. 65, no. 11, pp. 2844-2859, June 2017.
- [7] M. Masoudi et al., "Green mobile networks for 5G and beyond," *IEEE Access*, vol. 7, pp. 107270-107299, 2019.
- [8] A. Kaushik et al., "Joint bit allocation and hybrid beamforming optimization for energy efficient millimeter wave MIMO systems," *IEEE Trans. Green Commun. Netw.*, vol. 5, no. 1, pp. 119-132, Mar. 2021.
- [9] E. Vlachos et al., "Energy efficient transmitter with low resolution DACs for massive MIMO with partially connected hybrid architecture," *IEEE Veh. Tech. Conf. (VTC Spring)*, pp. 1-5, June 2018.
- [10] A. Kaushik et al., "Energy efficient ADC bit allocation and hybrid combining for millimeter wave MIMO systems," *IEEE Global Commun. Conf. (Globecom)*, pp. 1-6, Dec. 2019.
- [11] A. Hassaniien, et al., "Dual-function radar communication systems: A solution to the spectrum congestion problem," *IEEE Signal Process. Mag.*, vol. 36, no. 5, pp. 115-126, Sept. 2019.
- [12] B. Paul et al., "Survey of RF communications and sensing convergence research," *IEEE Access*, vol. 5, pp. 252-270, Dec. 2017.
- [13] C. B. Barnett, et al., "Full duplex radio/radar technology: The enabler for advanced joint communication and sensing," *IEEE Wireless Commun.*, vol. 28, no. 1, pp. 82-88, Feb. 2021.
- [14] A. Zhang, et al., "An overview of signal processing techniques for joint communication and radar sensing," *IEEE Jour. Sel. Topics Signal Proc.*, vol. 15, no. 6, pp. 1295-1315, Nov. 2021.
- [15] F. Liu et al., "Integrated sensing and communications: towards future dual-functional wireless networks," *IEEE Jour. Sel. Areas Comm.*, in press.
- [16] C. D. Ozkaptan et al., "Enabling communication via automotive radars: An adaptive joint waveform design approach," *Proc. IEEE Conf. Comp. Commun. (INFOCOM)*, pp. 1409-1418, 2020.
- [17] D. Ma et al., "Joint radar-communication strategies for autonomous vehicles: Combining two key automotive technologies," *IEEE Sig. Process. Mag.*, vol. 37, no. 4, pp. 85-97, July 2020.
- [18] F. Liu, et al., "MU-MIMO communications with MIMO radar: From co-existence to joint transmission," *IEEE Trans. Wireless Commun.*, vol. 17, no. 4, pp. 2755-2770, Apr. 2018.
- [19] A. Kaushik et al., "Waveform design for joint-radar communications with low complexity analog components," *IEEE Int. Symposium Joint Comm. Sensing*, pp. 1-5, Mar. 2022.
- [20] S. Chen et al., "Pre-scaling and codebook design for joint radar and communication based on index modulation," *arXiv:2111.10527*, pp. 1-4, Nov. 2021.
- [21] B. Clerckx et al., "Rate splitting for MIMO wireless networks: a promising PHY-layer strategy for LTE evolution," *IEEE Commun. Mag.*, vol. 54, no. 5, pp. 98-105, May 2016.
- [22] Y. Mao et al., "Rate-splitting multiple access for downlink communication systems: bridging, generalizing, and outperforming SDMA and NOMA," *EURASIP Jour. Wireless Commun. Netw.*, vol. 2018, no. 1, p. 133, May 2018.
- [23] H. Joudeh and B. Clerckx, "Sum-rate maximization for linearly precoded downlink multiuser MISO systems with partial CSIT: a rate-splitting approach," *IEEE Trans. Commun.*, vol. 64, no. 11, pp. 4847-4861, Nov. 2016.
- [24] B. Clerckx et al., "Rate-splitting unifying SDMA, OMA, NOMA, and multicasting in MISO broadcast channel: a simple two-user rate analysis," *IEEE Wireless Commun. Lett.*, vol. 9, no. 3, pp. 349-353, Mar. 2020.
- [25] Y. Mao et al., "Rate-splitting for multi-antenna non-orthogonal unicast and multicast transmission: Spectral and energy efficiency analysis," *IEEE Trans. Commun.*, vol. 67, no. 12, pp. 8754-8770, Dec. 2019.
- [26] Y. Cui et al., "Interference alignment based spectrum sharing for MIMO radar and communication systems," *IEEE Int. Workshop Sig. Process. Adv. Wireless Commun. (SPAWC)*, pp. 1-5, Jun. 2018.
- [27] Y. Zhao et al., "MIMO dual-functional radar-communication waveform design with peak average power ratio constraint," *IEEE Access*, vol. 9, pp. 8047-8053, 2021.
- [28] F. Liu, C. Masouros, A. P. Petropulu, H. Griffiths and L. Hanzo, "Joint Radar and Communication Design: Applications, State-of-the-Art, and the Road Ahead," *IEEE Trans. Commun.*, vol. 68, no. 6, pp. 3834-3862, June 2020.
- [29] A. Kaushik et al., "Dynamic RF chain selection for energy efficient and low complexity hybrid beamforming in millimeter wave MIMO systems," *IEEE Trans. Green Commun. Netw.*, vol. 3, no. 4, pp. 886-900, Dec. 2019.
- [30] A. Kaushik et al., "Energy efficiency maximization in millimeter wave hybrid MIMO systems for 5G and beyond," *IEEE Int. Conf. Commun. Netw. (ComNet)*, pp. 1-7, Oct. 2020.
- [31] E. Vlachos et al., "Radio-frequency chain selection for energy and spectral efficiency maximization in hybrid beamforming under hardware imperfections," *Proc. Royal Soc. A*, vol. 476, no. 2244, pp. 1-20, Dec. 2020.
- [32] A. Kaushik et al., "Energy efficiency maximization of millimeter wave hybrid MIMO systems with low resolution DACs," *IEEE Int. Conf. Commun. (ICC)*, pp. 1-6, May 2019.
- [33] A. Kaushik et al., "Hardware efficient joint radar-communications with hybrid precoding and RF chain optimization," *IEEE Int. Conf. Commun. (ICC)*, pp. 1-6, June 2021.
- [34] A. Kaushik et al., "Green joint radar-communications: RF selection with low resolution DACs and hybrid precoding," *IEEE Int. Conf. Commun. (ICC)*, pp. 1-6, May 2022.

- [35] C. Xu et al., "Rate-splitting multiple access for multi-antenna joint communication and radar transmissions," *IEEE Int. Conf. Commun. (ICC) Workshops*, Dublin, Ireland, pp. 1-6, June 2020.
- [36] C. Xu, et al., "Rate-splitting multiple access for multi-antenna joint radar and communications," *IEEE Jour. Sel. Topics Signal Proc.*, Early Access.
- [37] R. Cerna-Loli, O. Dizdar and B. Clerckx, "A rate-splitting strategy to enable joint radar sensing and communication with partial CSIT," *Proc. IEEE 22nd Int. Workshop Signal Proc. Adv. Wireless Commun. (SPAWC)*, 2021, pp. 491-495.
- [38] R. Cerna-Loli, O. Dizdar and B. Clerckx, "Rate-splitting multiple access for multi-antenna joint radar and communications with partial CSIT: precoder optimization and link-level simulations." *arXiv preprint arXiv:2201.10621*, 2022.
- [39] O. Dizdar et al., "Rate-splitting multiple access for joint radar-communications with low-resolution DACs," *IEEE Int. Conf. Commun. (ICC) Workshop*, pp. 1-6, June 2021.
- [40] D. R. Fuhrmann and G. San Antonio, "Transmit beamforming for MIMO radar systems using signal cross-correlation," *IEEE Trans. Aerospace Elec. Syst.*, vol. 44, no. 1, pp. 171-186, Jan. 2008.
- [41] M. Skolnik, "Radar handbook." McGraw-Hill Professional, 3rd ed., 2008.
- [42] A. Khawar et al., "Target detection performance of spectrum sharing MIMO radars," *IEEE Sensors Jour.*, vol. 15, no. 9, pp. 4928-4940, Sept. 2015.
- [43] A. Garcia-Rodriguez et al., "Reduced switching connectivity for large scale antenna selection," *IEEE Trans. Commun.*, vol. 65, no. 5, pp. 2250-2263, May 2017.
- [44] D. Ha et al., "Energy efficiency analysis with circuit power consumption in massive MIMO systems," *Proc. IEEE 24th Annual Int. Symp. Pers., Indoor, and Mobile Radio Commun. (PIMRC)*, 2013, pp. 938-942.
- [45] E. Björnson et al., "Optimal design of energy-efficient multi-user MIMO systems: is massive MIMO the answer?," *IEEE Trans. Wireless Commun.*, vol. 14, no. 6, pp. 3059-3075, June 2015.
- [46] S. Boyd et al., "Distributed optimization and statistical learning via the alternating direction method of multipliers," *Found. Trends Machine Learning*, vol. 3, no. 1, pp. 1-122, 2011.
- [47] W.-K. Ma, "Semidefinite relaxation of quadratic optimization problems," *IEEE Signal Proc. Mag.*, vol. 1053, no. 5888/10, 2010.
- [48] Y. Wang et al., "Global convergence of ADMM in nonconvex nonsmooth optimization," *J. Sci. Comput.*, 78, 29-63, 2019.
- [49] Z. Luo et al., "Semidefinite relaxation of quadratic optimization problems," *IEEE Signal Proc. Mag.*, vol. 27, no. 3, pp. 20-34, May 2010.
- [50] Y. Sun et al., "Majorization-minimization algorithms in signal processing, communications, and machine learning," *IEEE Trans. Signal Proc.*, vol. 65, no. 3, pp. 794-816, Feb.1, 2017.
- [51] G. Y. Li et al., "Energy-efficient wireless communications: tutorial, survey, and open issues," *IEEE Wireless Commun.*, vol. 18, no. 6, pp. 28-35, Dec. 2011.
- [52] J. Choi et al., "Joint user selection, power allocation, and precoding design with imperfect CSIT for multi-cell MUMIMO downlink systems," *IEEE Trans. Wireless Commun.*, vol. 19, no. 1, pp. 162-176, Jan. 2020.
- [53] J. An et al., "Rate-splitting multiple Access for multi-antenna broadcast channel with imperfect CSIT and CSIR," in *Proc. IEEE Annu. Symp. Pers. Indoor Mobile Radio Commun. (PIMRC)*, 2020, pp. 1-7.
- [54] F. Liu and C. Masouros, "Hybrid beamforming with sub-arrayed MIMO radar: enabling joint sensing and communication at mmWave band," *IEEE Inter. Confe. Acoustics, Speech Signal Proc. (ICASSP)*, pp. 7770-7774, 2019.
- [55] I. Bekkerman and J. Tabrikian, "Target detection and localization using MIMO radars and sonars," *IEEE Trans. Signal Proc.*, vol. 54, no. 10, pp. 3873-3883, Oct. 2006.
- [56] A. Shapiro et al., *Lectures on Stochastic Programming: Modeling and Theory*. Philadelphia, PA, USA: SIAM, 2009.
- [57] A. Papoulis and S. U. Pillai, "Probability, random variables, and stochastic processes." McGraw-Hill, Boston, 2002.